Agreement INGV-DPC 2007-2009

Project S4: ITALIAN STRONG MOTION DATA BASE

Responsibles: Francesca Pacor, INGV MIlano – Pavia
and Roberto Paolucci, Politecnico Milano

http://esse4.mi.ingv.it

Deliverable # D8

Identification of ITACA sites and records with distinctive features in their seismic response

May 2009

edited by:

UR3 Roberto Paolucci, Politecnico di Milano

UR2 Antonio Rovelli, INGV - Rome

Contributors

UR1 – INGV Milano

Gabriele Ameri, Dino Bindi, Ezio D'Alema, Sara Lovati, Lucia Luzi, Marco Massa, Giancarlo Monachesi, Francesca Pacor, Vera Pessina, Rodolfo Puglia

UR2 – INGV Roma

Fabrizio Cara, Carola Di Alessandro, Giuseppe Di Giulio, Giuliano Milana, Antonio Rovelli.

UR3 – Politecnico di Milano

Silvia Giorgetti, Roberto Paolucci, Chiara Smerzini, Marco Stupazzini

UR5 – Università della Basilicata

Rocco Ditommaso, Maria Rosa Gallipoli, Marco Mucciarelli

UR8 – GFZ Potsdam

Stefano Parolai, Marco Pilz

Table of contents

1. Introduction

The scope of the research activity within Task 4 is to clarify to which extent the records in the ITACA database may be affected by distinctive features in their seismic response. Such distinctive features may be due to various causes, such as:

- a complex geological and/or morphological environment that may cause earthquake ground motion amplification or deamplification in selected period ranges, and that is not usually accounted for in the standard site classification schemes;
- an earthquake source with directivity effects, high/low stress drops, shallow/deep hypocenter which may lead to ground motions amplitudes well beyond/below the standard dispersion bands for a group of recording stations;
- the interaction of the recording stations with the hosting structure or near-by structures, with narrow-band amplification effects at the natural vibration frequencies of the structure.

The identification of a subset of ITACA stations where such distinctive features are clearly highlighted is expected to improve the quality of available information in the dataset. For instance, identification of stations lying in large closed-shape alluvial basin will make more rationale the selection of accelerograms for engineering applications in similar geological conditions. Similarly, the end-user should be aware of records obtained in rock conditions, but where the topography or the lateral geological heterogeneities may strongly affect the seismic response.

To pursue the objectives of this Task, the following activities have been planned, that will be described in the chapters of this Deliverable.

(a) Analysis of strong motion records, to check whether the observed peak values at the same station, or for the same event, lie systematically beyond (or below) the average trend lines obtained by Empirical Ground Motion Predictive Equations (EGMPEs). To this end, new EGMPE calibrated on the Italian dataset will be described in *Chapter 2*, that will form the basis of both the specific activity for identification of anomalous records/stations described in *Chapter 3*, and of the site classification studies of the Task 5 of this Project (see Deliverable D12).

(b) Geomorphology study, aimed at the selection of stations located in complex geological features, such as deep alluvial basins, with possible site amplification effects at long periods, topographic irregularities, alluvial fans, or complex soil layering with velocity inversions. The preliminary activity for this purpose, mainly based on GIS data analyses, will be the object of *Chapter 4*.

(c) Identification of stations with possible significant interaction effects with the hosting or surrounding structures (*Chapter 5*).

(d) In-field monitoring activity, involving the seismic instrumentation of several ITACA station sites with complex geological configurations, such as steep topographic profiles and shallow/deep basins (*Chapter 6*).

(e) Numerical modelling using up-to-date tools for 2D-3D seismic wave propagation and soil-structure interaction analyses, that is expected to contribute to understand the physical reasons

of the distinctive features of seismic response at the selected sites, and the period range in which they mostly affect earthquake ground motion (*Chapter 7*).

As an annex of this Deliverable, the file Table_Task4.xls has been uploaded in the web site of Project S4 where most of the findings of the research activities included in this Deliverable have been summarized (see Annex A for a synthesis of the contents of this file). The final goal is to further summarize these findings within the ITACA stations monographs, where the space for a short description of the possible distinctive features of seismic response of the station has been included.

2. Reference attenuation relationships

2.1 Scope

For the purposes of Task 4, there is a need for predictive equations that well represent the variability of strong motions contained in ITACA. To reach this goal, two different approaches have been adopted. A first one follows the conventional scheme of the paper by Sabetta and Pugliese (1996), with a similar formalism and site classification, but enlarging the data set to include all the earthquakes with $M_w > 4$, for a total number of 106 earthquakes. An attempt to include the faulting style has been performed as well. The other approach, never applied so far to the Italian data set, uses a different formalism and different site classification. According to Fukushima et al. (2007), the dependence on distance is expressed by two terms and site classification is based on the predominant period of sites. This criterion is used in Japan for the seismic design of highway bridges (Japan Road Association, 1980 and 1990). Since the predominant period at a site is related to the ratio between the sediment thickness and velocity, it represents a combination of the traditional Vs30 criterion with the bedrock depth, implicitly introducing one more important parameter for the site classification. Zhao et al. (2006) describe an exhaustive application of this approach to a huge amount of data in Japan. The predictive equations derived in this deliverable will be also used in Task 5, where the performance of alternative site classification techniques will be checked, with particular attention to low cost methods such as spectral techniques using available strong/weak motion records.

2.2 New attenuation relationships based on Italian records

2.2.1 INGV-RM approach: site classification based on predominant period

In an approach aimed at checking the performance of a site classification based on site predominant period (Task 5), we have formulated new predictive equations adopting the functional form of Fukushima et al. (2007):

$$\log_{10} Sa(T) = a(T) + b(T)\, M + c(T)\, M^2 + d(T)\, R - \log_{10}(R + e(T)\, 10^{f(T)M}) + S_j(T)\delta_j \quad (2.1)$$

where Sa(T) is the elastic response spectral acceleration for 5% damping, M and R are moment magnitude and hypocentral distance (in km), respectively; a, b, c, d, e and S_j, are period-dependent regression coefficients. The suffix $_j$ corresponds to the seven site classes we propose on the basis of the predominant period. $S_j(T)\delta_j$ represents the individual site terms of stations and δ_j is a dummy variable, which is equal to 1 if data are observed at *j-th* site category accordingly to the site classification and 0 otherwise.
We classify each site by assigning one of the seven predominant period classes that we introduce (in the range 0.05 to 2 seconds) as a modification of the Zhao et al. (2006) approach (Table 2.1).

Table 2.1 Different classifications based on site predominant-period of response spectra.

Site Class Zhao et al. (2006)	Site Class Fukushima et al. (2007)	Site Class Our proposal	Site Natural Period T (s)
SC-I Tg < 0.2 s	SC-1 Tg < 0.2 s	CL-I	Tg < 0.2 sec.
SC-II 0.2 ≤ Tg < 0.4 s	SC-2 0.2 ≤ Tg < 0.6 s	CL-II	0.2 ≤ Tg < 0.4 s
SC-III 0.4 ≤ Tg < 0.6 s		CL-III	0.4 ≤ Tg < 0.6 s
SC-IV Tg ≥ 0.6 s	SC-3 Tg ≥ 0.6 s	CL-IV	Tg ≥ 0.6 s
-----	SC-4 Tg not estimable but site originally classified as rock	CL-V	Tg not estimable (flat H/V)
-----	SC-5 Tg not estimable but site originally classified as soil	CL-VI	broad amplification / multiple peaks Tg > 0.2 s
-----	-----	CL-VII	Tg not estimable (multiple peaks over entire period range)

The predominant period is identified from the average horizontal-to-vertical spectral ratios of the 5%-damped response spectra of records (Figure 2.1). We selected a data-set of 602 three-component analogue and digital recordings from 120 earthquakes recorded at 214 seismic stations within a hypocentral distance of 200 km. We selected events in the M_W range of 4.0 to 6.8 and in the focal depth ranges from 5 to 40 km (Di Alessandro et al., 2008).

In Figure 2.2 a comparison is shown between our predictive equations and others based on predominant site periods, for 50 km of hypocentral distance and Mw 5.0, 6.0 and 6.8 (from the bottom to the top). In general all curves display a good agreement; some differences in classification criterion among the different predictive equations, however, may lead to some not significant discrepancies.

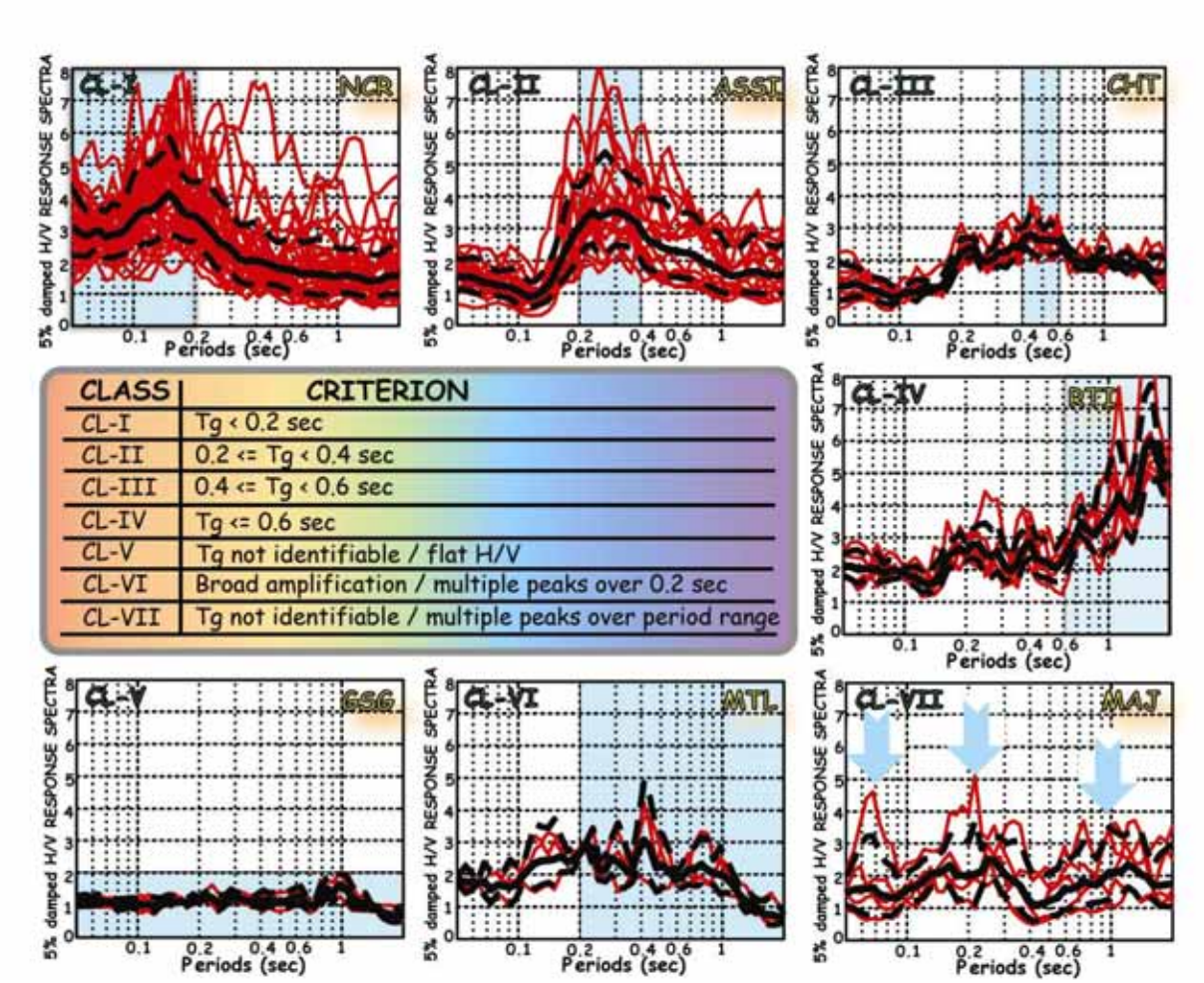

Figure 2.1 Proposed classification criterion based on the predominant period identified from the average H/V spectral ratio (black solid line) of the 5%-damped response spectra recorded at each site (red curves). The first four classes (CL-I to CL-IV) are defined using the same criterion of Zhao et al. (2006), according to the period band (blue area) where the predominant peak occurs. Further three classes take into account stations that could not be classified as a function of a unique peak: CL-V displays an almost flat average H/V response spectral ratio (< 2), CL-VI has a broad amplification at periods longer that 0.2 s or multiple peaks at periods longer than 0.2 s (blue arrows), CL-VII has multiple peaks both before and after 0.2 s, therefore the station cannot be unambiguously classified.

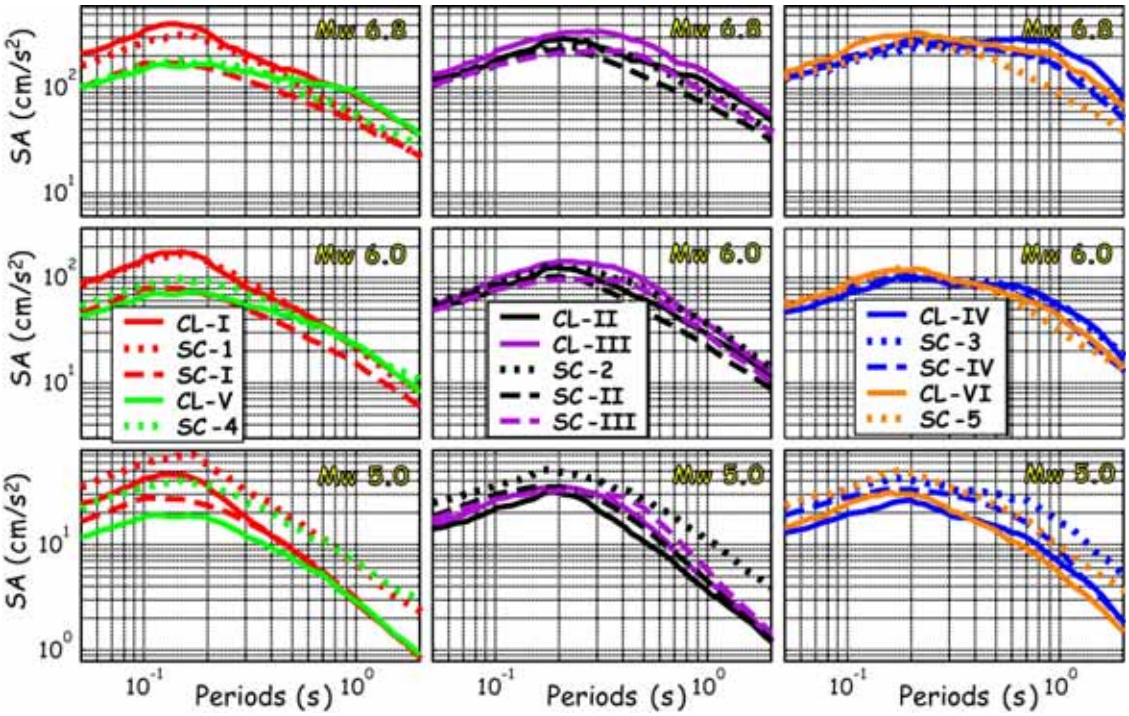

Figure 2.2 Comparison of predicted response spectra for Mw 5.0, 6.0 and 6.8 and hypocentral distance 50 km, according to different EGMPEs based on site predominant-period classes (see Table 2.1). Sites that amplify at short periods or have a rock -like behaviour are shown in the left panel, sites that amplify at intermediate periods or have a shallow-soil - like behaviour are shown in the central panel and sites that amplify at long periods or have a deep-soil - like behaviour are shown in the right panel.

2.2.2 INGV-MI approach: site conditions based on SP96 classification

Data

These EGMPEs (denoted hereinafter as ITA08) have been calibrated using the strong motion data collected in the ITACA database (http://itaca.mi.ingv.it/), i.e., 106 earthquakes with moment magnitude larger than or equal to 4 and distances from the fault smaller than 100 km and recorded by at least two stations. In addition, the waveforms recorded by the RAIS network (http://rais.mi.ingv.it/), installed around the Garda lake area in Northern Italy have also been considered, consisting of three earthquakes occurred in 2006 and 2007, with magnitudes in the range 4.2 – 4.5. Figure 2.3 shows the distribution of stations (left) and earthquakes (right), as well as the magnitude-distance scatter plot.
Since a detailed geophysical characterization is available only for a small subset of sites, the stations were grouped according to the site classifications used in Sabetta and Pugliese (1987), consisting of three classes. The first class (hereinafter referred to as C_0) includes the stations installed on rock; the second class (C_1) includes the stations installed on shallow sediments (thinner than 20 m) while the third class (C_2) is representative of the stations installed on sediments thicker than 20m, where with the term "sediment" are denoted soils with shear wave velocity lower than 800 m/s.

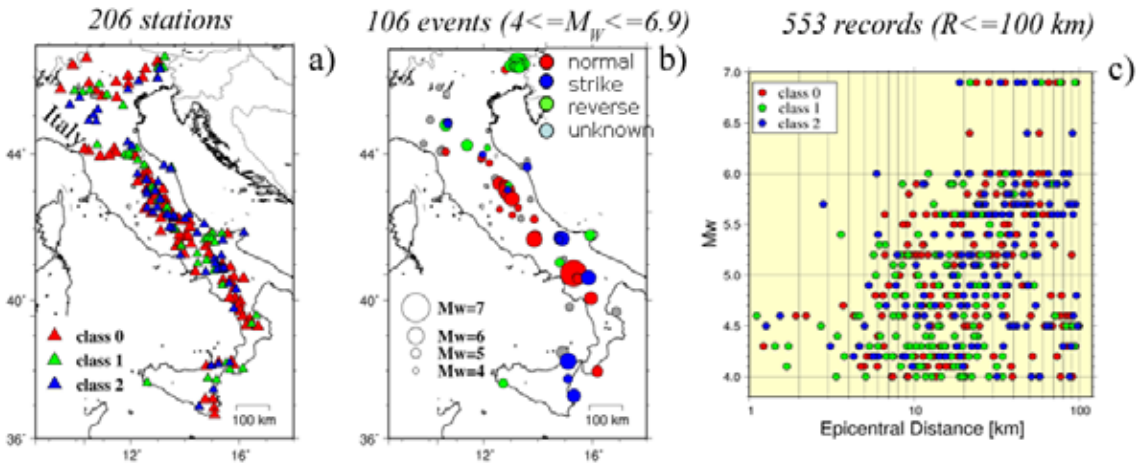

Figure 2.3 Strong motion stations (left) and earthquakes (middle) considered to derive the ITA08 EGMPE. The stations (triangles) are classified accordingly to the scheme proposed by Sabetta and Pugliese (1987). The magnitude-distance (Joyner-Boore distance) scatter plot relevant to the recordings considered to develop ITA08 is shown in the right panel.

Model

ITA08 has been developed considering the following predictive functional model:

$$\log_{10} Y = a + b_1(M_W - 4.5) + b_2(M_W - 4.5)^2 + (c_1 + c_2(M_W - 4.5))\log_{10}\sqrt{(R_{JB}^{\ 2} + h^2)} + e_i S_i \quad (2.2)$$

where Y is the response variable; R_{jb} is the Joyner-Boore distance if M≥5.5, otherwise the epicentral distance is adopted; h is the pseudo-depth (km); S_i , with i=1,2,3, are dummy variables equal either to 0 or 1 depending on soil type (rock, class C_0: S_1=1 and S_2=S_3=0; shallow alluvium, class C_1: S_2=1 and S_1=S_3=0; deep alluvium, class C_2: S_3=1 and S_1=S_2=0; e_i are the site coefficients. The regressions were performed for the maximum horizontal (maxH) and vertical peak ground (V) acceleration (PGA) and velocity (PGV), as well as for 5%-damped spectral acceleration (SA) at 21 periods from 0.03 to 2 sec.
A regression scheme based on the random effect model (Brillinger and Preisler, 1985; Abrahmson and Youngs, 1992) was adopted to describe the errors which are assumed to be independent and normally distributed. The inter-event and inter-station distributions of errors are used to identify stations or earthquakes with peculiar behavior (see Chapter 3).

Results

Figure 2.4 shows the computed site coefficients for maxPGA, as a function of period. The results confirm that class 1 mainly includes stations with amplifications at frequencies higher than 5 Hz, while the amplification for class 2 is stronger frequencies lower than 2Hz.

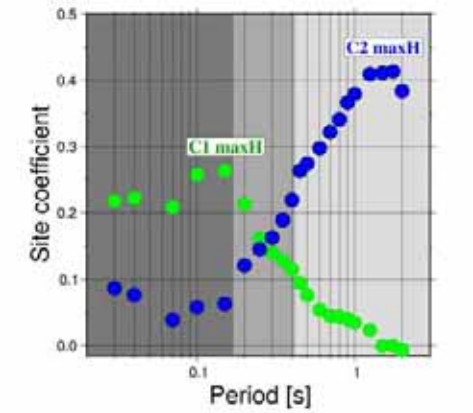

Figure 2.4 Site coefficients e_1 (class C1) and e_2 (class C2) for maxPGA.

Figure 2.5 summarizes results for the spectral acceleration values predicted at rock sites for two distances (20 and 50 km) and two magnitude values (6.5 and 5.5). The predictions from ITA08 are compared with the European model of Ambraseys et al (2005). A general good agreement is observed, with the main differences in the high frequency range. Finally, the comparison for PGV shown in Figure 2.6,highlights the tendency of ITA08 to underestimate the ground motion at distances shorter than 10 km with respect to global models.

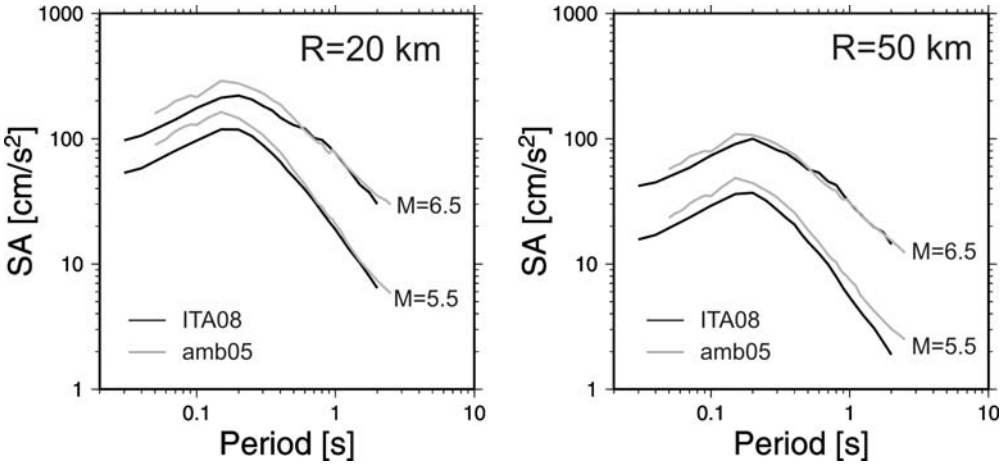

Figure 2.5 Comparison between the spectral acceleration predicted at rock sites (class C0) by ITA08 and the European model proposed by Ambraseys et al (2005). Two magnitudes (6.5 and 5.5)

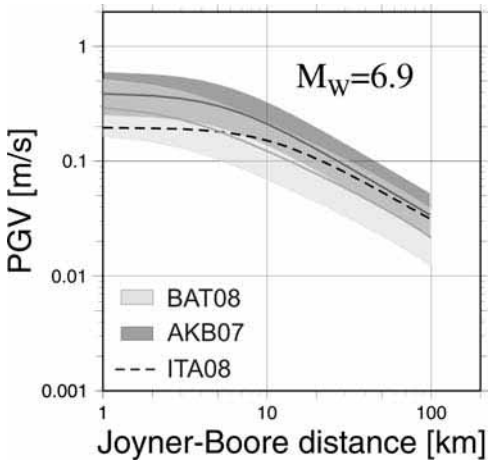

Figure 2.6 Peak ground velocity predicted for a magnitude 6.9 at rock site: comparison with Boore and Atkinson (2008) and Akkar and Bommer (2007).

2.2.3 Comparison between the proposed approaches

Finally, in order to compare the results of the proposed approaches, we display in Figure 2.7 the results of the EGMPEs evaluated for M_w 6.0 at 50 km hypocentral distance.

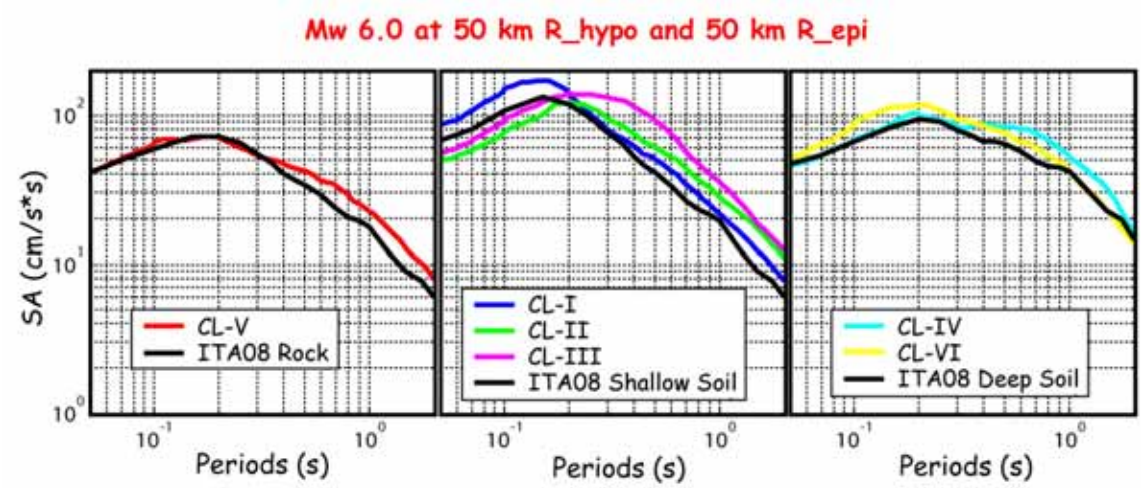

Figure 2.7 Comparison of predicted response spectra for Mw 6.0 at a general distance of 50 km, according to ITA08 and the equation proposed in 2.2.1, based on site predominant-period classes.

As a further comparison, we have plotted in Figure 2.8 the predictions by the two GMPEs presented in this Deliverable for a Mw6.3 event, corresponding to the Ap3r 6 L'Aquila earthquake. It turns out that a large part of observations falls within the statistical uncertainty interval of both equations. It is interesting to note that values lower than expected, below -1 sigma, correspond to stations NW of the epicenter, probably due to their anti-directive position. As a matter of fact, preliminary evaluations of the source rupture of the L'Aquila mainshock support a significant directivity toward SE (N.A. Pino, private communication).

2.3 References

Bindi, D., Luzi, L., Massa, M. and Pacor, F. (2009). "Horizontal and vertical ground motion prediction equations derived from the Italian Accelerometric Archive (ITACA)," submitted to *Bull. Earth. Eng.*

Di Alessandro, C., Bonilla, L.F, Rovelli, A. and O. Scotti (2008). Influence of site classification on computing empirical ground-motion prediction equations in Italy, in the 2008 AGU Fall Meeting, San Francisco, CA, USA, 15-19 December 2008, paper n. S12A-05.

Fukushima Y., Bonilla L. F., Scotti O., Douglas J. (2007). Site classification using horizontal-to-vertical response spectral ratios and its impact when deriving empirical ground-motion prediction equations, J. Earthq Eng., 11, 712-724.

Japan Road Association (1980). Specifications for Highway Bridges Part V, Seismic Design, Maruzen Co., LTD.

Japan Road Association (1990). Specifications for Highway Bridges Part V, Seismic Design, Maruzen Co., LTD

Sabetta, F., and A. Pugliese (1996). Estimation of response spectra and simulation of nonstationary earthquake ground motions, Bull Seism. Soc. Am. 86, 337 - 352.

Zhao, J. X., K. Irikura, J. Zhang, Y. Fukushima, P. G. Somerville, A. Asano, Y. Ohno, T.

Oouchi, T. Takahashi and H. Ogawa (2006), An Empirical Site-Classification Method for Strong-Motion Stations in Japan Using H/V Response Spectral Ratio, Bull. Seism. Soc. Am., 96, 914-925.

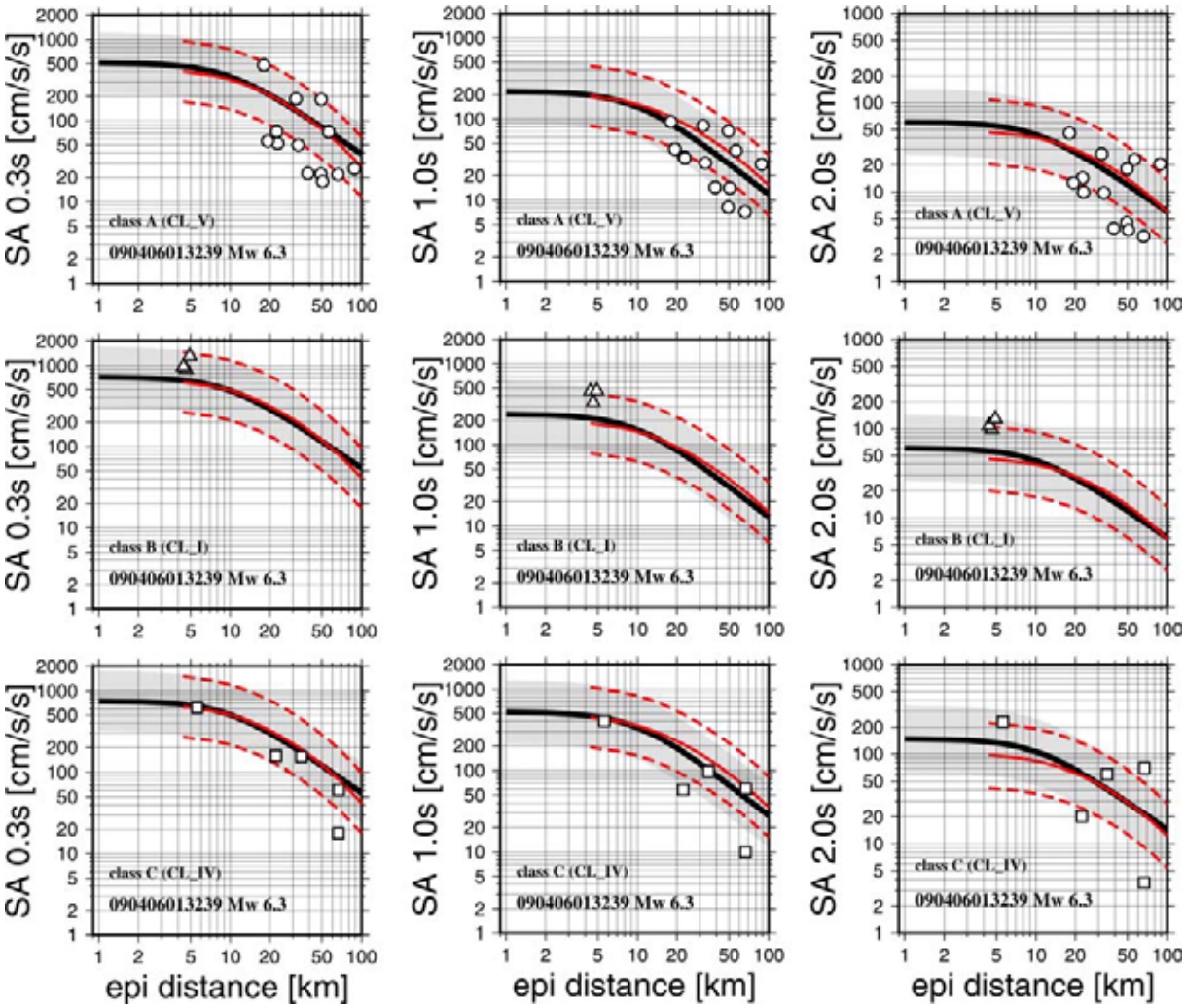

Figure 2.8 Comparison between GMPEs presented in this Deliverable: the black curves denote the median ±1 s.d. ITA08 predictions (par. 2.2.2), while the red curve denote the ones by INGV-RM (par. 2.2.1). Magnitude is M_W 6.3. Spectral ordinates (at 0.3, 1 and 2 sec, from the left to the right side of the figure) are those of stations that recorded the April 6, 2009, L'Aquila earthquake. Open circles, triangles and squares represent different site classes (in top, middle and bottom panels, respectively).

3. Analysis of strong motion records

3.1 Scope

The objective of this chapter is to identify which stations or which earthquake events exhibit a distinctive trend so that the recorded peak values of ground motion, typically in terms of 5% damped response spectral ordinates, fall above or below the standard dispersion bands of the attenuation relationships calibrated on the Italian data (see Chapter 2).
Figure 3.1 sketches, in terms of Peak Ground Acceleration values, the main aim of this work.

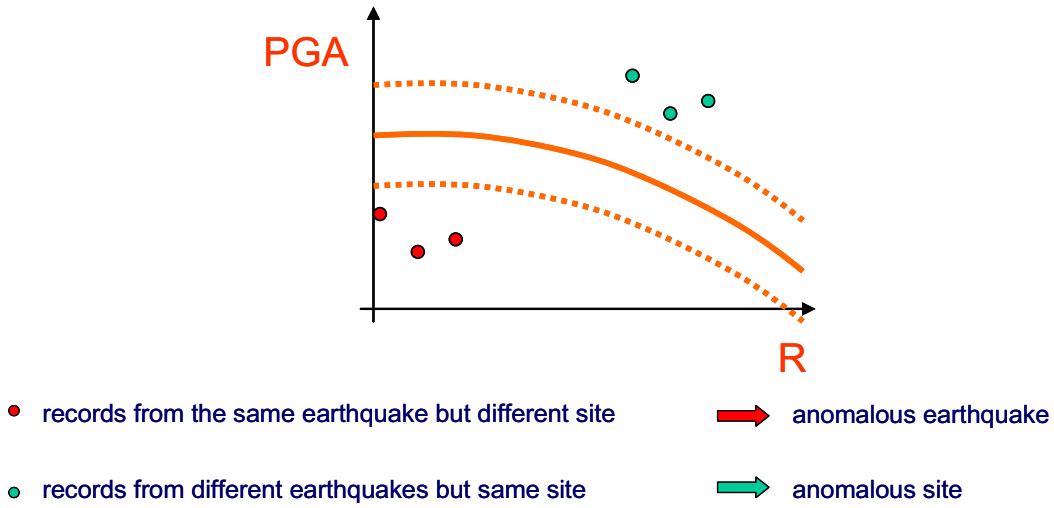

Figure 3.1. Sketch of possible anomalous features of seismic response, either due to distinctive features of the station response, or due to distinctive seismic source effects.

Records of a single station from different earthquakes may fall above the standard deviation band of the EMPGE (green dots in Figure 3.1): this suggests that either the station is wrongly classified or its classification is accurate but the recorded ground motion exceeds the standard dispersion band, owing either to a complex geological configuration not accounted for in the site classification, or to station-structure interaction effects that show themselves in a specific period range. On the other side, records from a single earthquake and different stations may fall below the standard dispersion band: this suggests a distinctive feature of the seismic event, possibly due to forward/backward directivity effects, an anomalous high/low stress drop, or an anomalous shallow/deep earthquake focus.

Based on the need, highlighted in the previous Chapter, to calibrate on the ITACA records different EGMPE with different classification schemes, two approaches have been devised with the common aim to extract the anomalous records as sketched in Figure 3.1. The ongoing activity and the results of both approaches, will be summarized in the Table of Annex A of this Deliverable. Such results will be cross-checked with those of other approaches, such as the geomorphology study outlined in *Chapter 4* and the station-structure interaction study of *Chapter 5*, with the objective to eventually highlight in the ITACA database only those cases that meet different identification criteria.

3.2 INGV-RM approach

To assess to what extent each record is "different" from its statistical expectation and to judge if site behaviour or source is responsible for the "difference", station-to-station and event-to-event variability are computed using the empirical attenuation relation discussed above in 2.3.2.
We adopt the premises that Abrahamson and Youngs (1992) described for their mixed model, assuming that, while deriving an empirical ground motion prediction equation, we can commit an error that can be a combination of fixed effects (i.e. whose estimate from all the dependencies can be considered) and a random effect (for which we do not estimate explicitly the dependency on all the data). According to them, the overall error can be partitioned into two parts: the inter-event and intra-event terms.
An attenuation regression model has the form:

$$ln\, y_{ij} = f(M_i, r_{ij}, \theta) + \varepsilon_{ij} + \eta_i \qquad (3.1)$$

where y_{ij} is a ground motion parameter, $f(M_i, r_{ij}, \theta)$ is the attenuation equation, M is the earthquake magnitude, r is the distance, θ is a vector of model parameters, ε_{ij} is the error term of the jth recording from the ith event and represent the intra-event variations, and η_i represent the inter-event variations. η_i and ε_{ij} are assumed to be independent, normally-distributed variants with variances σ^2 and τ^2, respectively.
For each period, to derive estimates of η_i and ε_{ij}, we use a maximum likelihood formalism borrowed from Spudich et al. (1999), who in their turn adapted the maximum likelihood method of Joyner & Boore (1993) to the problem of determining the mean value of the residuals (the bias) and its standard deviation. The residuals are evaluated with respect to the *ad hoc* computed regression (2.1) using the predominant period. Figure 3.2 shows the estimated values of the over-all standard deviation, as well as the inter- and intra-event variations as a function of period.

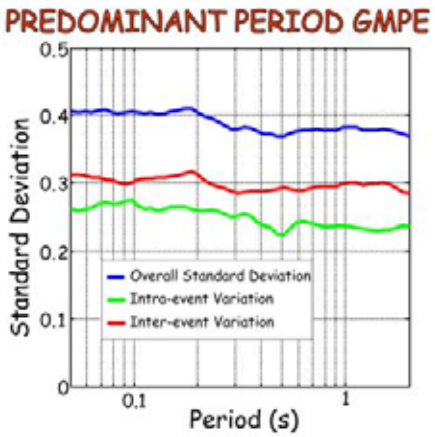

Figure 3.2 Plots of overall, inter-event and intra-event variations as derived from the maximum-likelihood approach adapted from Spudich et al. (1999) and Joyner & Boore (1993) to the proposed predominant period classification.

According to the mixed effect model, the maximum likelihood solution for the random effects η_i (event-to-event variation) is given by:

$$\eta_i(T) = \frac{\tau^2 \sum_{j=1}^{n_i} (y_{ij} - \mu_{ij})}{n_i \tau^2 + \sigma^2} \tag{3.2}$$

where μ_{ij} is the predicted value as function of M_i, r_{ij} and θ, and n_i is the number of records from the *i*th event .

Plots of η_i for the individual events included in the database used to derive the attenuation regression equation provide the opportunity to evaluate the presence of some events with distinctive features, as characterized by larger (or smaller) values with respect to predicted values. For this purpose, we plot the values of 10^(ηi) for 6 selected periods (PGA, 0.1 sec, 0.2 sec, 0.5 sec, 1.0 sec and 2.0 sec) for all the 120 events in our database, evaluating the discrepancy of the values from the unity (see Figure 3.3). Note that high or low values can be related to various reasons, among which poor determinations of moment magnitude or hypocentral parameters, relevant influence of recordings from station with distinctive amplification features or anomalously large or small stress drop for some events.
To evaluate the presence of stations with distinctive amplification characteristics, for each record we remove the influence of the individual event term variation from the computed residual values, and then we average the so corrected residuals for each station.
Stations characterized by distinct amplification patterns are the ones whose absolute average residuals exceed the value 1.65 σ (where σ is the station-to-station deviation), corresponding to a confidence interval of 90%.
Among the 111 stations included in the database, we find the presence of 17 stations exceeding the proposed threshold of the intra-event variation. Figure 3.4 shows the absolute average residuals (blue curves) and 1 standard deviation interval (red curves) for the recognized “peculiar” 17 stations. In each graph it is possible to recognize the station code, the classification based on predominant period criteria (see Table 2.1) and the cumulative absolute value of station exceedance with respect to the chosen threshold value of 1.65 (thick black dotted lines). Stations are ordered on the basis of their predominant period class and subsequently with alphabetical order.
Finally, we notice that there is no clear connection between classes and the intervals where the stations average residuals exceed the threshold. Within a certain extent, it seems that stations located on deep soft soil or basins (i.e. class CL-IV), that are known to amplify low frequencies, tend to attenuate high frequencies. This is expected but never emerged so clear using other predictive equations. In Figure 3.4 we can recognize distinctly this behaviour in stations SELI, AQI, AQK, and SCV, that underestimates high frequencies up to - 1 sigma.

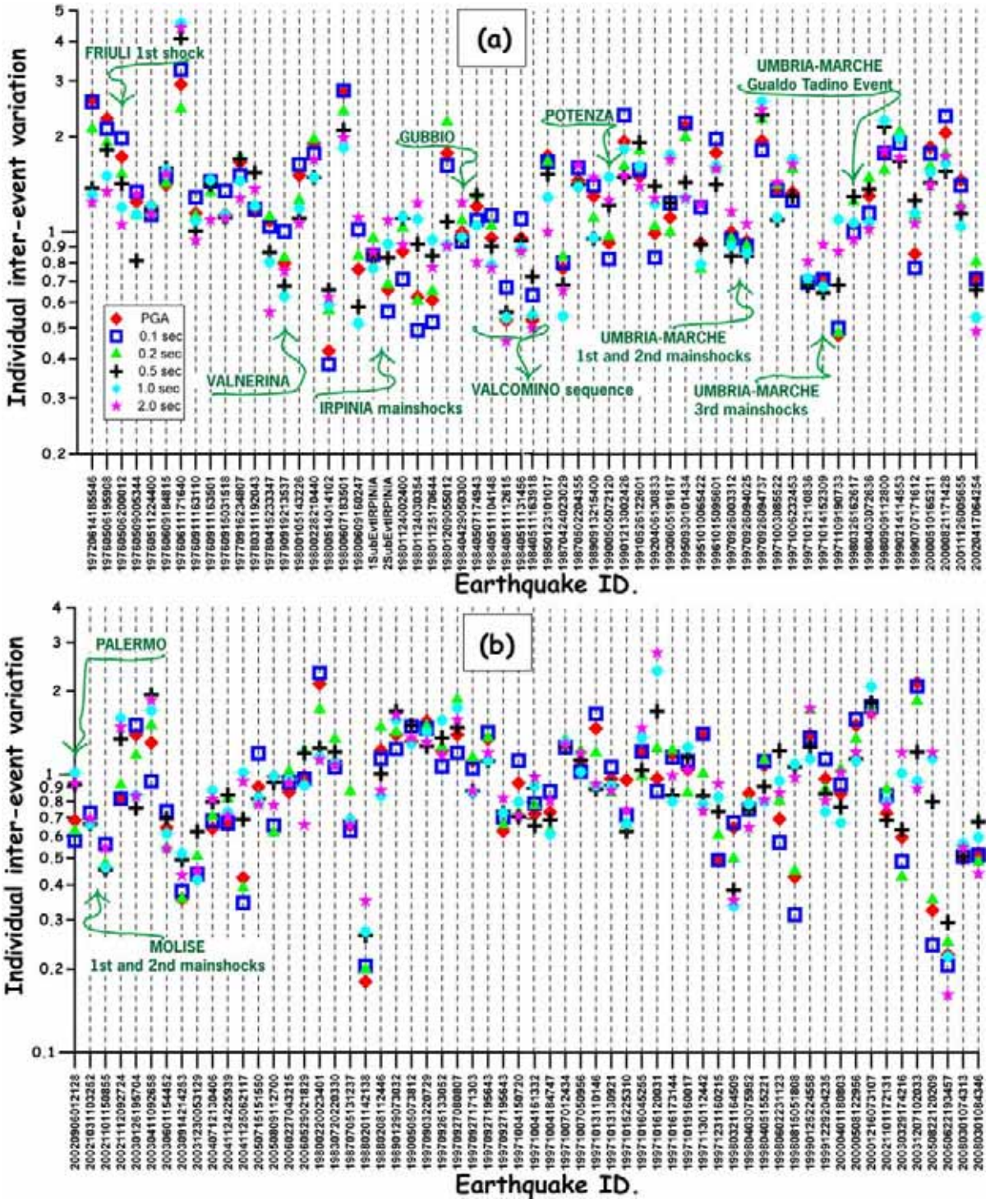

Figure 3.3 Plots of the individual inter-event variations for selected periods and for the events included in the analyzed dataset. The ID. of the earthquake provide a reading key for the events' date and time. Selected famous Italian earthquakes are highlighted with special arrows, together with their denomination.

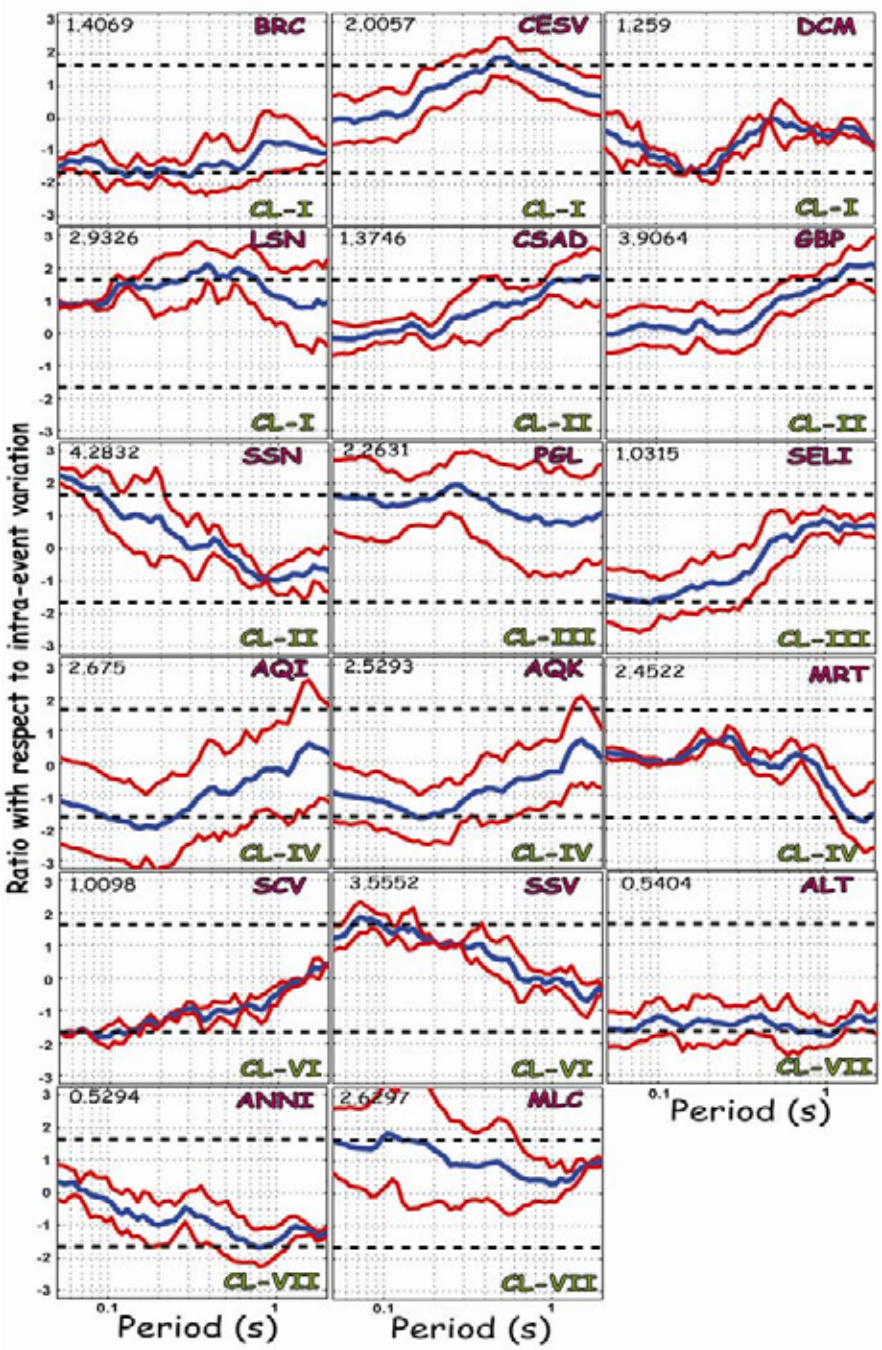

Figure 3.4 Absolute average residuals (±1 Standard deviation) for the 17 stations characterized by distinct amplification patterns as they exceed 1.65 times the computed intra-event variation (also known as the station-to-station deviation).

3.3 INGV-MI & POLIMI approach

3.3.1 Introduction

We present herein an empirical procedure to identify strong motion stations characterized by distinctive features and to quantitatively assess their effects on recorded earthquake ground motions. The method consists of computing the residuals of the recorded 5%-damped response spectral acceleration with respect to the estimate provided by ITA08 (section 2.2) as a function of period (0.03s $\leq T \leq$ 2s). This procedure allows one to identify in a systematic

way strong motion stations showing significant deviations from the average behavior expected for their class in a statistical way.

3.3.2 Dataset

The dataset used for the study reported in this section is the same used by Bindi et al. (2009b) to derive ITA08, consisting of N_r 553 strong motion recordings relevant to a total number N_E=106 earthquakes with moment magnitude M_W varying from 4.0 to 6.9 and recorded at epicentral distances up to about 100 km (see Figure 2.3). The considered sites (total number N_S=206) have been initially classified using the soil classification proposed by Sabetta and Pugliese (1996), where Vs30 has been introduced for sake of clarity.

1) rock sites with V_{S30} > 800 m/s (C_0, 100 stations);
2) shallow alluvial deposits with thickness smaller than 20 m and 400 m/s < V_{S30} < 800 m/s (C_1, 48 stations);
3) deep alluvial deposits thicker than 20 m and V_{S30} < 400 m/s (C_2, 58 stations).

Only earthquakes with at least two recordings have been selected while it was not possible to follow the same criterion for the strong motion stations, otherwise too many stations of potential interest would have been excluded from the dataset. Specifically, the number of recordings for each earthquake varies from 2 (e.g. 1972 M_W 4.8 Ancona earthquake) to 24 (1997 14 October M_W 5.6 Umbria-Marche earthquake), while the number of recordings for each stations varies from 1 (for 70 stations) up to 23 (for the station Nocera-Umbra2 - NCR2).

3.3.3 Proposed method: calculation of residuals

As the goal of this work is the identification of strong motion stations showing distinctive features which deviate significantly form the average behavior, as predicted by the common empirical ground motion models, the analysis has been carried out station by station. In other words, for each of the 206 stations considered in this analysis, the residuals between the measured and predicted logarithmically-transformed spectral accelerations $SA(T)$ at 21 periods from T=0.03 s to T=2s are analyzed. The analysis is period-dependent, thus allowing one to study the dependence of variability of earthquake ground motion on the considered spectral range.
The residual $r_{p,q}(T)$ for the p^{th} station and the q^{th} event is defined as:

$$r_{p,q}(T) = Log\left[SA_{p,q}^{obs}(T)\right] - Log\left[SA_{p,q}^{GMPE}(T)\right] \qquad \text{for } p = 1...N_S,\ q = 1...N_E \tag{3.3a}$$

where $SA_{p,q}^{obs}(T)$ and $SA_{p,q}^{GMPE}(T)$ are, respectively, the observed and predicted spectral acceleration for the station p and earthquake q. Subsequently, it was decided to normalize the residuals computed as follows:

$$r_{p,q}^{N}(T) = \frac{r_{p,q}(T)}{\sigma^{GMPE}} \tag{3.3b}$$

where σ^{GMPE} is the logarithmic standard deviation of the selected EGMPE. Note that behind Equations (3.3a) and (3.3b) there is the assumption that measured ground motions are approximately normally distributed, hypothesis that is generally fulfilled (see e.g. Bommer et al. 2004; Douglas and Gehl, 2008).

To compute the residuals, the empirical attenuation law recently developed by Bindi et al. (2009b) and calibrated on the same dataset was considered throughout the work. For the normalization according to (3.3b), it was decided to consider the inter-station error, i.e. $\sigma^{GMPE} = \sigma_{sta}$, rather then the total standard deviation. Further details about this aspect will be given below. This choice is dictated by the fact that it permits to take into account easily the site conditions (C=0, 1 and 2), since information about V_{S30} is not yet available for all the strong motion stations and the EGMPE adopts the same soil classification. Correction of residuals for local site conditions is particularly useful because it allows to highlight the stations for which the recorded $SA(T)$ is remarkably different from the median value expected for their class (either rock or shallow alluvium or deep alluvium), rather than a relative amplification/deamplification with respect to rocklike conditions. The results of the residual analysis may present some bias due to the fact the dataset coincides with that used to derive the EGMPE. Nevertheless, it was verified that results are robust with respect to the empirical model used. An example of the sensitivity analysis with respect to the EGMPEs will be illustrated later on (see Figure 3.7).
One of the main advantages of the procedure presented herein is, in fact, that it can be easily extended to other empirical ground motion models (e.g. NGA).

Correction for inter-event variability

Referring to Joyner and Boore (1993) for a more detailed overview on the methods for regression analysis of earthquake ground motion data, it has become common practice when deriving EGMPEs to divide the aleatoric variability (σ) into the inter-event and intra-event variability. In some cases, as for the EGMPE by Bindi et al. (2009b), the latter is further separated into the inter-station (σ_{sta}) and record-to-record variability (σ_{rec}). Starting from the consideration of these different components of ground motion variability, residuals have been corrected for the inter-event variability, as follows:

$$R^N_{p,q}(T) = r^N_{p,q}(T) - \varepsilon_q(T) \quad \text{with} \quad \varepsilon_q(T) = \frac{\sum_{k=1}^{N_q} r^N_{k,q}(T)}{N_q} \quad \text{for } q = 1...N_E \tag{3.4}$$

where $\varepsilon_q(T)$ quantifies the error associated with the q^{th} earthquake, computed as the average normalized residual over the N_q records from the same earthquake. The correction (3.4) turns out to be quite relevant in deriving unbiased residuals, when records from the same event share source-specific distinctive features. As an illustrative example, Figure 3.5a show the inter-event error for each earthquake of the dataset for SA at T=0.03 s (left) and at T=1s (right). For instance, the large positive error for the 1972 M_W 4.8 Ancona earthquake (Event ID #1) at zero or very small periods may be attributed to the propagation efficiency of the Adria micro-plate (Castro et al., 1999), which caused exceptionally large PGAs. The significant under-estimation of the 1990 M_W 5.6 Easter Sicily earthquake may be due to the uncertainties on the source-site distance and magnitude (Bindi et al., 2009a). The low level of shaking observed for the M_W 5.7 2002 Molise shocks, Oct. 31 and Nov. 1 (Event ID #90 and #91), is well captured by the inter-station errors, which tend to stabilize on negative values regardless of the considered period (see Figure 3.5b).
Finally, for each station p the median and 16°-84° percentiles are computed from all the recordings available for the same site.
Figure 3.6 illustrates the corrected residuals for three representative stations: Montefiegni Fiastra- MNF located on rock (C_0), Peglio - PGL on shallow alluvium (C_1) and Rieti- RTI on deep alluvium (C_2). The filled dots denote the median values while the vertical bars denote the 16° and 84° percentiles calculated on the set of recordings available for each station. It is

apparent from the corresponding maps that the distinctive trends may be due to particular local configurations: for instance, the large negative value for the station MNF over the whole period range 0.03 s – 1 s is likely due to the complex topography and to the proximity to the Fiastra dam while the large positive residuals observed at long periods (T>~0.5-0.6 s) for the RTI station is clearly due to the generation of surface waves inside the alluvial basin.
It is worth underlining that the reliability of the results obtained with this procedure strongly depends on the number of available recordings for each station: the procedure may be critical for those stations with only one recording and has to be checked against other data.

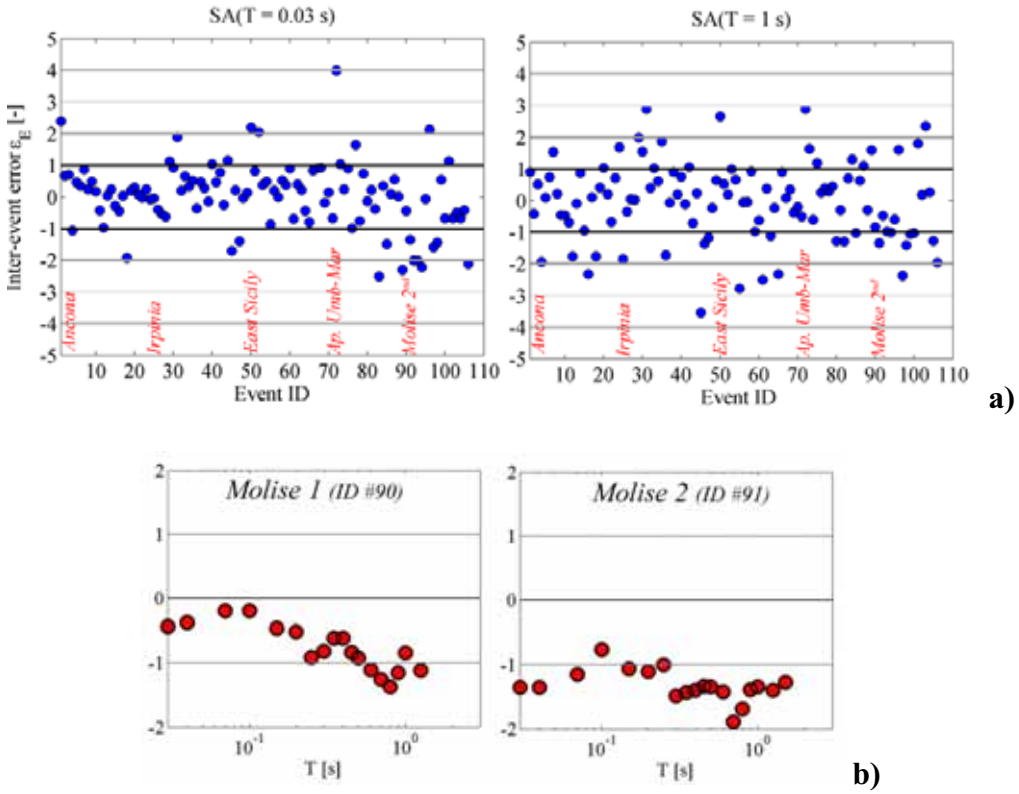

Figure 3.5 a) Inter-event errors, computed according to (3.4), for each earthquake of the dataset under consideration (N_E=106), for spectral acceleration at T=0.03 s (left) and T=1 s (right). b) inter-event error as a function of period for the M_W 5.7 Oct 31 Molise first shock (left) and M_W 5.7 Nov 1 Molise second shock (right).

To check the robustness of the results with respect to the empirical attenuation law, a sensitivity analysis with respect to the EGMPEs has been carried out. Figure 3.7 depicts the residues for the RIETI station (RTI) as a function of period obtained using four different empirical models: 1) Ambraseys et al. (2005); 2) Cauzzi & Faccioli (2008); 3) Boore & Atkinson (2008) and Bindi et al. (2009b). The residues are here computed with respect to "standard" conditions, i.e. assuming normal style of faulting and rock conditions. Although some differences in terms of magnitude of the residuals, results obtained from different EGMPEs reproduce the same trend with significant amplifications at large periods.

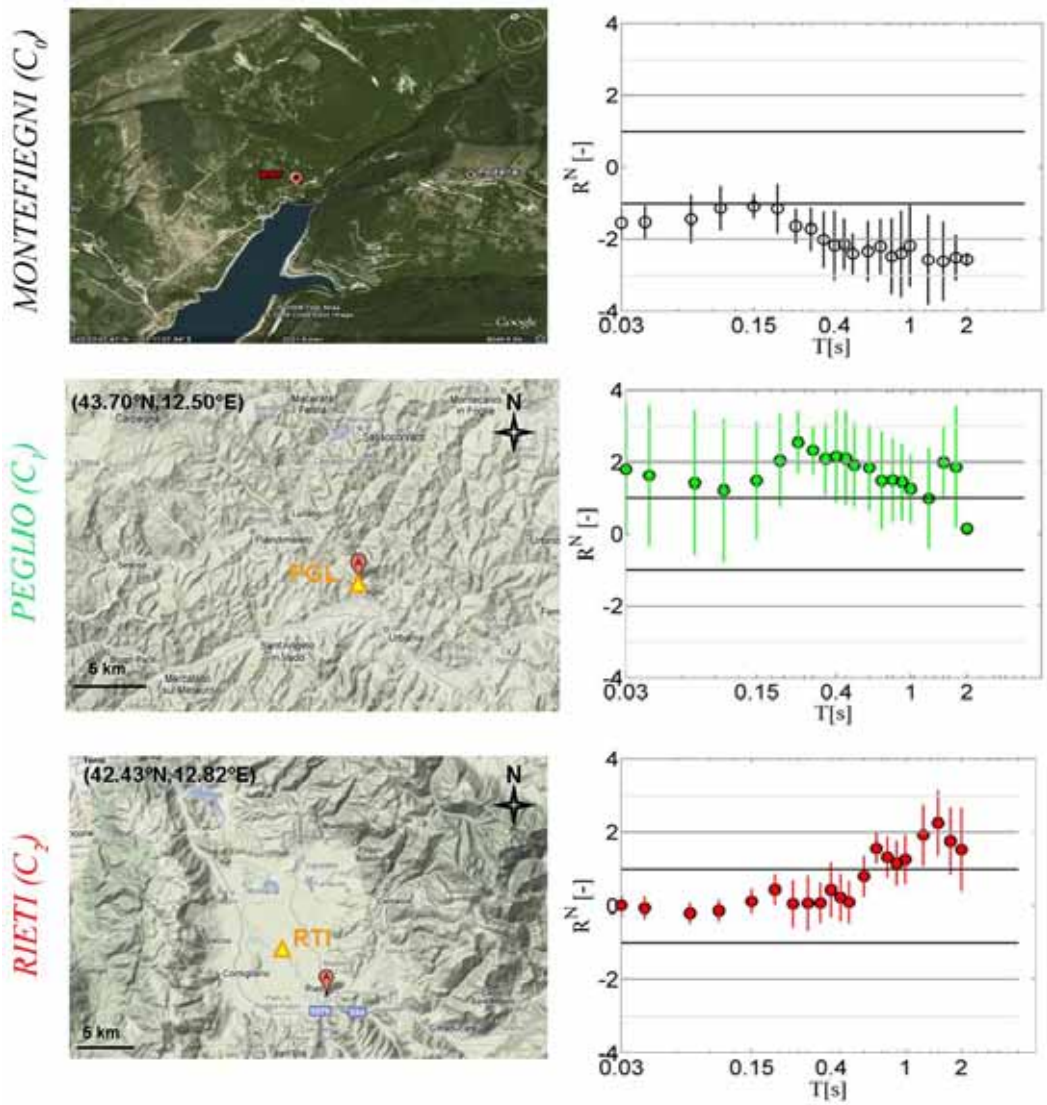

Figure 3.6 Residuals corrected for the inter-event variability for three representative stations: Montefiegni Fiastra- MNF located on rock (C_0, white), Peglio - PGL on shallow alluvium (C_1, green) and Rieti- RTI on deep alluvium (C_2, red). Filled dots indicate the median value, while the vertical bars denote the 16°-84° percentiles.

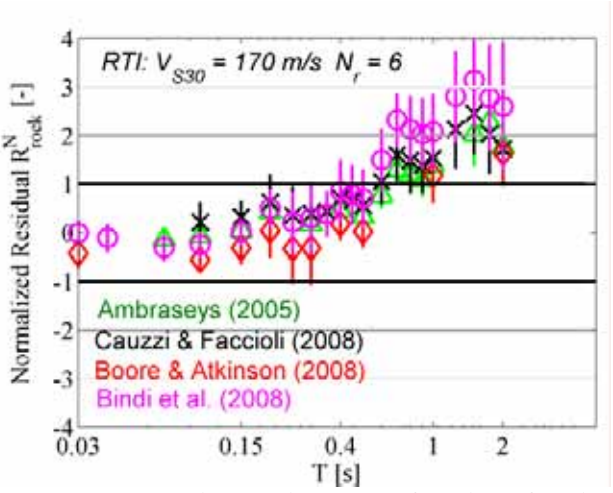

Figure 3.7 Comparison between the normalized residues as a function of period computed for the RIETI station (RTI) assuming different empirical ground motion models: Ambraseys et al. (2005), green triangles; Cauzzi & Faccioli (2008), black crosses; Boore & Atkinson (2008), red diamonds and Bindi et al. (2009b), magenta dots.

3.3.4 Results

To provide synthetic measures of the observed dependence of residues on period, it was decided to calculate, for each station, the average values in the following period ranges: i) 0.03s≤T≤0.15s; ii) 0.20s≤T≤0.40s; iii) 0.45s≤T≤1.0s and iv) 1.25s≤T≤2s. Results for the whole 206 stations under consideration in terms of average residues over the aforementioned period ranges are summarized in the file Table_Task4.xls, attached to this deliverable in the web site of Project S4 (see Annex A for a synthesis of the contents of this file).
Table 3.1 gives some statistics regarding the number of stations exceeding the threshold of 1.65σ for each soil class (C_0, C_1 and C_2). Note that for soil class 2, the largest percentage of stations with $R^N \geq 1.65\sigma$ occurs at long periods (1.25s≤T≤2s).
As an illustrative example, Figure 3.8 depicts the residues as a function of period for 9 representative stations exceeding the threshold of 1.65σ over at least one of the selected period ranges: 3 stations on rock, C_0 (Guardiagrele GRD, Naso NAS, Pescasseroli PSC), 3 on shallow alluvium, C_1 (Lesina LSN, Norcia NCR, Pennabilli PNN) and 3 on deep basin, C_2 (L'Aquila V. Aterno – Aquil. Park. AQK, Barisciano BRS, Scafa SCF) are reported. In each plot, the median value (filled dot) and the 16°-84° percentiles are given along with the average residues over the 4 period ranges (denoted by horizontal arrows). Note that this representation helps identifying easily either those stations which emphasize the behaviour of their class, i.e. amplification at short periods, T<~ 0.2, for SP=1 or amplification at long periods, T>~0.5s, for SP=2, or those stations which show distinctive trends which deviate from the expected behaviour of their class, e.g. with deamplification or amplification at periods not accounted for by the ground motion attenuation model.

Table 3.1 Number of stations exceeding the threshold of 1.65 σ over the selected period ranges for the different site classes.

	C_0 (100 stations)		**C_1 (48 stations)**		**C_2 (58 stations)**	
Period range	# stations	%	# stations	%	# stations	%
T_1: 0.03 - 0.15 s	3	3	2	4.2	4	6.9
T_2: 0.20 - 0.4 s	10	10	1	2.1	4	6.9
T_3: 0.45 - 1 s	8	8	2	4.2	5	8.6
T_4: 1.25 - 2 s	8	8	2	4.2	9	15.5

3.4 Preliminary indications and future developments

In this chapter, an original analysis has been proposed aiming at selecting stations from the ITACA dataset that mostly contribute to the dispersion of the EGMPE that have recently been proposed in the framework of this Project. The goal of this analysis is twofold. On one side, it may either point out stations that have been misclassified from the point of view of site conditions, or it may suggest criteria for improving seismic site classification, as planned within Task 5 of this Project. On the other side, related to the objectives of Task 4 this Deliverable is referring to, the selected station may fall outside the dispersion bands for any site classification criterion under consideration, so that it can be considered to show some distinctive features of site response, probably related to a complex geological configuration

(deep closed shape basin, steep topographic irregularity, etc.) not accounted for in the most common seismic site classification schemes.
For this reason, two EGMPEs have been proposed and considered in this study, that, although based essentially on the same dataset, are very different in terms of site condition description: the idea is that stations falling outside the dispersion bands of both equations may be highlighted as potentially affected by complex site effects.

The future developments, planned to complete the work described in this chapter, are summarized as follows:

i) Identification of stations falling outside the dispersion bands of both EGMEs considered and check of this information with the help of the geo-morphological criteria that will be introduced in the following Chapter 4.
ii) Specific detailed analysis of rock stations, in order to understand whether complex site effects related to topography, lateral discontinuities or hard vs. soft rock conditions may help to better discriminate the station seismic response
iii) Identification and list of anomalous seismic events within the ITACA database.

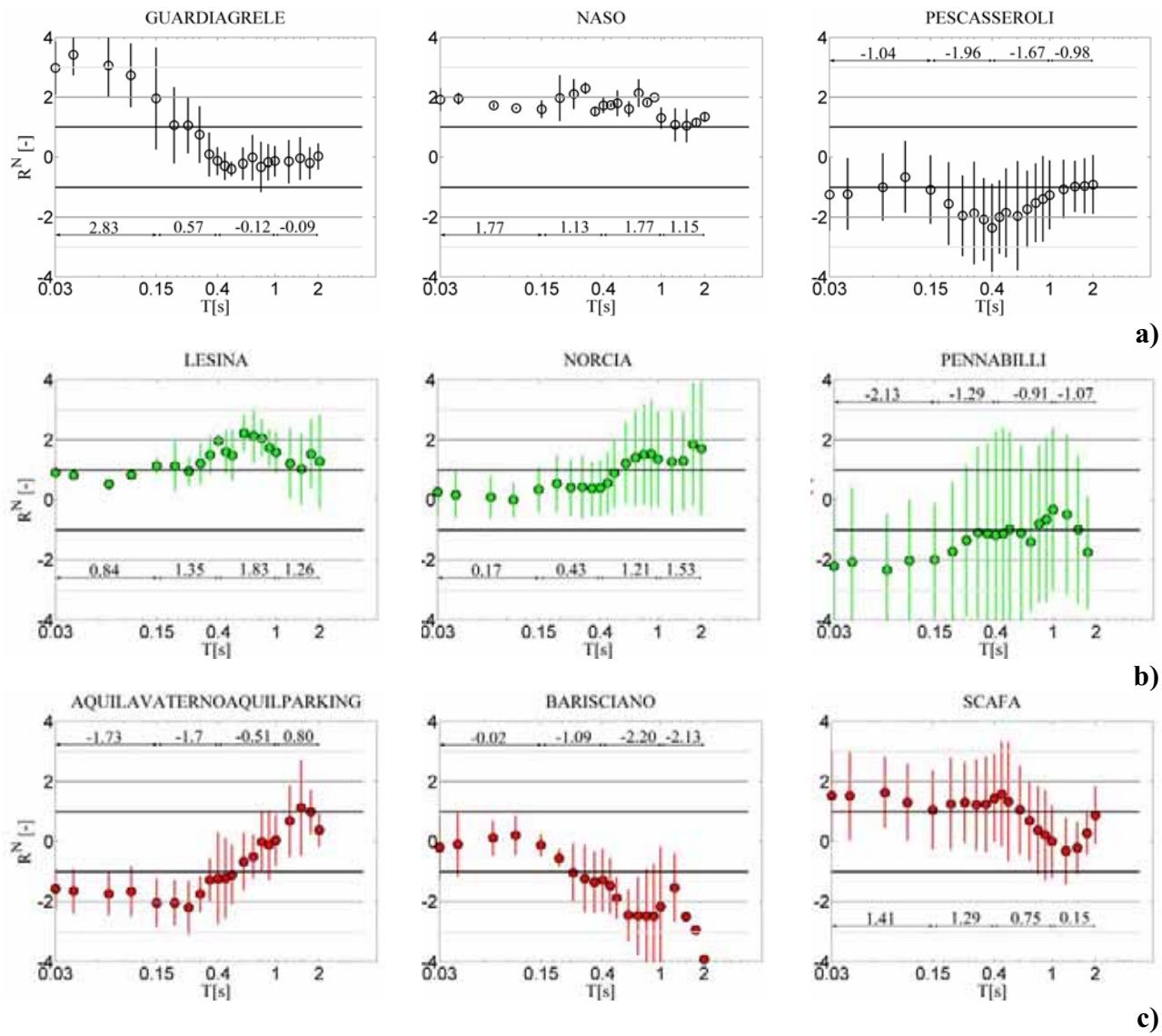

Figure 3.8 Residues as a function of period for 9 representative stations for soil class 0 (a), 1 (b) and 2 (c).

3.5 References

Abrahamson, N.A. and Youngs, R.R. (1992) "A stable algorithm for regression analyses using the random effects models, Bull. Seismol. Soc. Am., 82, 505-510.

Ambraseys, N. N., Douglas, J. and Sarma, S. K. (2005) "Equations for the estimation of strong ground motions from shallow crustal earthquakes using data from Europe and the Middle East: Horizontal peak ground acceleration and spectral acceleration," Bull. Earth. Eng., 3 (1), 1-53.

Bindi, D., Luzi, L. and Pacor, F. (2009a) "Inter-event and inter-station variability computed for the Italian Accelerometric Archive (ITACA),", Bull. Seismol. Soc. Am., accepted for publication.

Bindi, D., Luzi, L., Massa, M. and Pacor, F. (2009b) "Horizontal and vertical ground motion prediction equations derived from the Italian Accelerometric Archive (ITACA)," submitted to *Bull. Earth. Eng*.

Bommer JJ, Abrahamson NA, Strasser FO, Pecker A, Bard PY, Bungum H, Cotton F, Fäh D, Sabetta F, Scherbaum F, Studer J (2004) "The challenge of defining upper bounds on earthquake ground motions," Seismol Res Lett, 75(1), 82–95.

Boore, D.M. and Atkinson, G.M. (2008) "Ground-Motion Prediction Equations for the Average Horizontal Component of PGA, PGV, and 5%-Damped PSA at Spectral Periods between 0.01 s and 10.0 s," Earthquake Spectra, 24 (1), 99-138.

Castro, R.R., Mucciarelli, M., Monachesi, G., Pacor, F. and Berardi, R. (1999) "A review of nonparametric attenuation functions computed for different regions of Italy," Annali di Geofisica, 42, 735-748.

Cauzzi, C. and Faccioli, E. (2008) "Broadband (0.05 to 20 s) prediction of displacement response spectra based on worldwide digital records," Journal of Seismology, DOI 10.1007/s10950-008-9098-y

Douglas, J. and Gehl, P. (2008) "Investigating strong ground-motion variability using analysis of variance and two-way-fit plots," Bull. Earth. Eng., 6, 389–405.

Joyner, W.B. and Boore D.M. (1993) "Methods for regression analysis of strong-motion data," Bull. Seismol. Soc. Am.," 83 (2), 469–487.

Sabetta, F. and Pugliese, A. (1996) "Estimation of Response Spectra and Simulation of Nonstationary Earthquake Ground Motions," Bull. Seismol. Soc. Am., 86(2), 337-352.

Spudich, P., Joyner, W. B, Lindh, A. G., Boore, D. M., Margaris, B. M. and Fletcher, J. B. (1999) "A Revised Ground Motion Prediction Relation for Use in Extensional Tectonic Regimes," Bull. Seismol. Soc. Am., 89 (5), 1156-117.

4. Identification of stations based on geo-morphological criteria

4.1 Scope

Strong amplification of earthquake ground shaking are often attributed to deep basins and topographic irregularities, such as observed in Italy during the Friuli (Brambati et al. 1980), Irpinia (Sirovich, 1982), Umbria-Marche (Pacor et al. 2006) and Molise earthquakes, or deduced by historical observations, as in the case of 1887 Western Liguria earthquake (Faccioli et al. 2002). A comprehensive study of deep basin amplification effects in Italy was recently carried out within the S5 Project "Seismic input in terms of expected spectral displacements" (INGV - DPC 2004 – 2006), while, following the work by Paolucci (2002), a first attempt for the identification on a regional scale of urban centers on topographic relieves prone to significant amplifications effects was carried out in a recent Master Thesis (Davì, 2008).
The identification of morphological structures able to amplify seismic ground motion can be performed by Geographic Information Systems (GIS), through morphometric analyses. High resolution digital terrain models (DEM) and geological data are the main input of these analysis that are performed at regional scale, typically. An important source of data is represented by the digital cartographic "Karita" database (http://kharita.rm.ingv.it/dmap/).
The scope of this activity within Project S4 is twofold. On one side, the information coming from the geo-morphological study will be cross-checked with the identification of stations with anomalous peak values of recorded response, as studied in *Chapter 3* of this Deliverable, to verify the compatibility of results coming from both approaches. On the other side, the geo-morphological characterization will be used to improve the station site description and classification, as available from the station monographs to be compiled under Task 2.

4.2 Stations within closed-shape deep basins

4.2.1 Identification of stations lying on deep basins

In the last INGV-DPC research programme (2004 – 2006), the influence of alluvium filled basins on displacement response spectra was investigated in the S5 Project (http://progettos5.stru.polimi.it/Index.html), and a preliminary version of amplification basins map was presented by Vanini et al. (2007) (Figure 4.1). The map illustrates all valleys and basins with a minimum dimension of 500 m, capable to amplify the displacement response spectra at long period. Basins were identified assuming that both conditions of *flat zone* and *soil presence* are simultaneously verified. GIS analyses have been performed using a DEM (Digital Elevation Model) at 7.4" resolution, and geological data (1:500.000 scale) to identify and classify the areas of the Italian Peninsula with potential "basin effects".

Starting from the map of Figure 4.1, the selection criteria adopted in this Project for identification of basins with potential distinctive features in their seismic response, especially in the long period range, were further constrained, and limited to *closed-shape* basins with *width-to-length ratio* sufficiently large (say > 0.15) At the present stage, a quantitative formulation of these criteria was not deemed to be relevant, and the identification has been made on a "visual" basis.

Figure 4.1 Amplification basins map elaborated in the S5 Project - Seismic input in terms of expected spectral displacements (DPC – INGV 2004-06)

Two important considerations have to be made:

- in the present work, some geological formations have been reclassified, with respect to the version of the map in Figure 4.1;
- some open basins, not too elongated, fronting the Tyrrhenian sea, could be included in the present classification, as soon as evidences of ground motion amplification are found (this could be the case of the Gioia Tauro basin in Calabria, the Eboli and Castel Volturno ones in Campania, The Grosseto basin in Toscana and the Catania one in Sicilia).

The resulting map is illustrated in Figure 4.2 referring to Central Italy, where most relevant closed-shape basin structures are located.

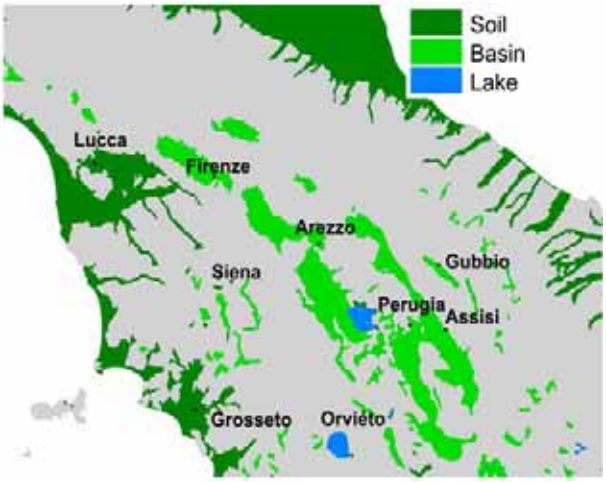

Figure 4.2 Example of closed-shape basin map in Central Italy.

A selection of such basins, supported by the strong motion observations of long period amplifications, is shown in Figure 4.3, regarding the cases of Rieti, Norcia, Avezzano and Gubbio. The investigation of these case-studies, once a more detailed geological map (1:100.000) and additional information will be available in the second year project, is expected to provide a relationship between a simplified geometric characterization of the basin (for example in terms of shape regularity, average depth, W/L ratio, local heterogeneity, etc.) and the intensity and period range of surface waves induced by the basin itself.

Note that long period amplifications as shown in Figure 4.3 are not exclusive of stations lying inside deep alluvial basins that can be pointed out in a straightforward way by this approach. Probably the most important station from this point of view is L'Aquila Aquilpark (AQK, see Fig. 3.8, bottom left), located downtown in one of the most damaged part of the city. L'Aquila lies on stiff alluvial material overlying softer olocenic lacustrine deposits, at the edge of the Aterno Valley. Although surface geology would have suggested a seismic response proper of stiff soils, the intensity of long period ground motion is probably governed by the depth of lacustrine sediments, that, under L'Aquila, are supposed to reach their maximum depth down to about 250 m (De Luca et al., 2005). This clearly points to the need of a cross-validation of both approaches illustrated in this report, i.e., the one based on the residual analysis and the one based on surface geo-morphology.

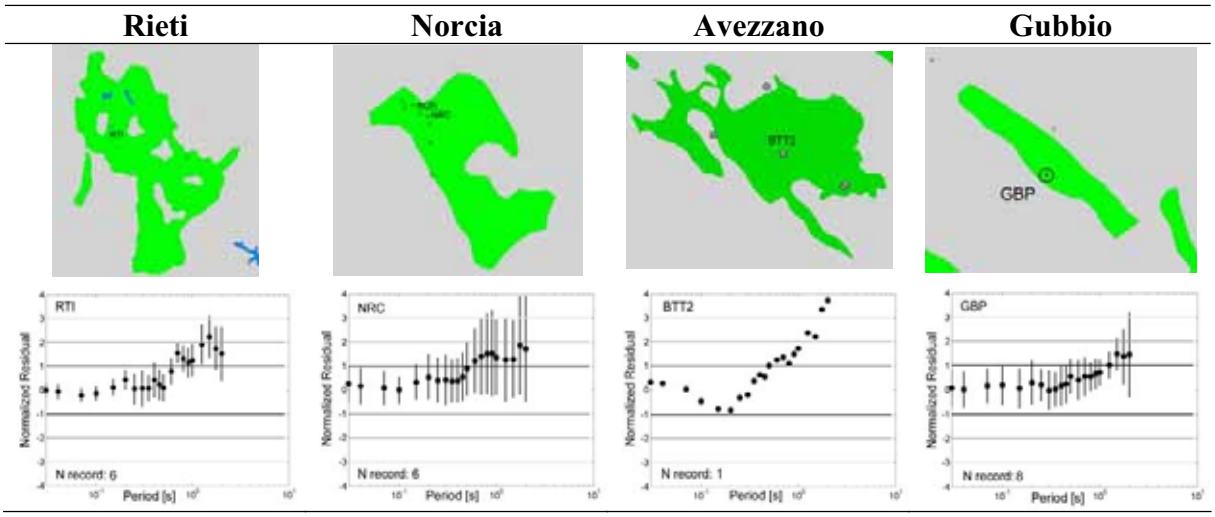

Figure 4.3 Basins with evidence of long period amplification effects. on the lower side of the figure the residuals with respect to the median EGMPE for stations lying inside the basin are reported.

4.2.2 Identification of recording stations on deep closed-shape basins

A preliminary attempt to identify ITACA stations located in basins, was made by the intersection through GIS between the *basins* and *stations* layers. A buffer of 500 m was calculated for each station with the aim of resolving the following problems:

(i) the station coordinates may not be accurate
(ii) basins are identified on a 1:500.000 scale, with rough detail level
(iii) georeference of stations may not be fully accurate

The results of the intersection are illustrated in Table 4.1.

Table 4.1 Results of the intersection between *basins* and *stations* layers

Total stations	Station intersecting basins	Station completely inside a basin	Station intersecting no-basin conditions in a 500 m ray
616	112	65	47

The last group of stations (#47) needs a special check in order to exclude georeferencial problems, rough basin classification of just to verify their position on the edge of the basin. A more detailed geological information (1:100.000) will subsequently be used.

For instance, the exact location of Assisi station (ASS), on a basin classification at 500.000, corresponds to a deep basin. However, since its 500 m buffer intersects a no-basin area (Figure 4.4, left), the improvement of detail available from a 1:100.000 geological map allows one to to correctly locate Assisi station on stiff soil ("Formazione della scaglia rossa-bianca") (Figure 4.4, centre), at the beginning of the slope surrounding the plain basin (Figure 4.4, right).
For the moment, only stations completely inside basins have been considered, although classification of stations at basin edges would be of much interest as well.

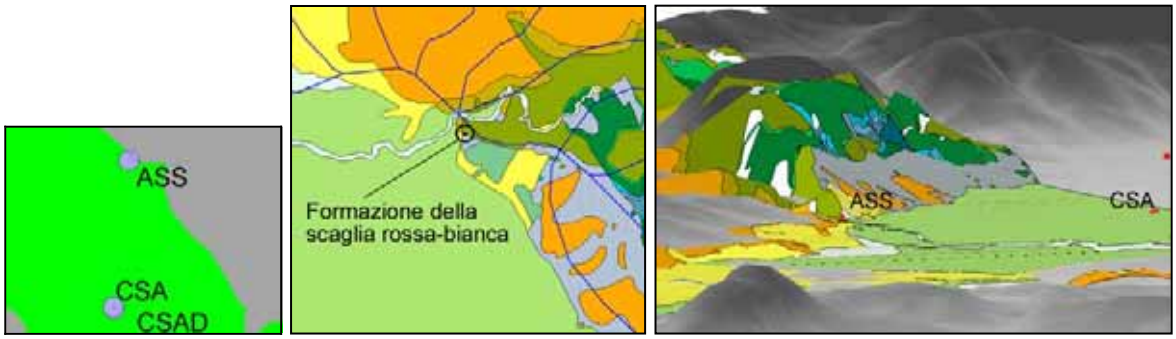

Figure 4.4 Location of the ASS station on a basin classification map at 1:500.000 scale , with buffer of 500m (left), and same location on a geological map at 1:100.000 scale, with high definition of the soil formations (right). DEM of the Assisi basin surrounded by relieves

4.3 Stations on steep topographic sites

4.3.1 Topographic amplification phenomena

Topographic amplification of seismic waves may be related to (i) focusing of seismic waves on a locally convex surface profile, or (ii) to a dynamic phenomenon that produces the resonant motion of the whole hill.
The Italian and European seismic codes suggest coefficients of topographic amplification in the 1 – 1.4 range, depending on the morphology of the relief. Essentially they are based on 2D numerical analyses and are therefore properly applicable only to crests and elongated ridges (Italian Technical Norms NTC 2008; Eurocode 8, Part 5). According to the norms, the morphology parameters to identify potentially amplifying topographic irregularities are (i) the average slope i (with limit values of 15° and 30°) and (ii) the height of the relief (H > 30 m). However, the definition of topographic categories are affected by some ambiguity (e.g. i = "average slope" or "relief characterized by top-width significantly less than the base-width"), so that the attribution of a topographic relief to one class or the other is not straightforward. Recently, the Italian technical guidelines "Indirizzi e criteri per la microzonazione sismica" (2008) suggest the use of graphs based on more restrictive parameters (i > 10° e H > 10 m).

4.3.2 Proposed approach and examples

By GIS technology, and thanks to the DEM availability (20x20m or 100x100m resolution) for all national territory, it is nowadays possible to classify it into layers of topographic classes, and to verify to which class one station belongs.
From the DEM, the slope can be easily calculated by GIS and subsequently classified in the critical ranges of inclination (< 15°, 15°-30° and > 30°). On the other hand, the identification of a valley and of a ridge is a more complex procedure, but it can similarly be generalized at national scale. Once the valley and the ridge have been identified, the height of the relief (H > 30 m) can be subsequently calculated as the difference of elevation between ridge and valley.

Figure 4.5 shows the scheme of the ridge-valley conditions (left) and the resulting GIS analysis (right).

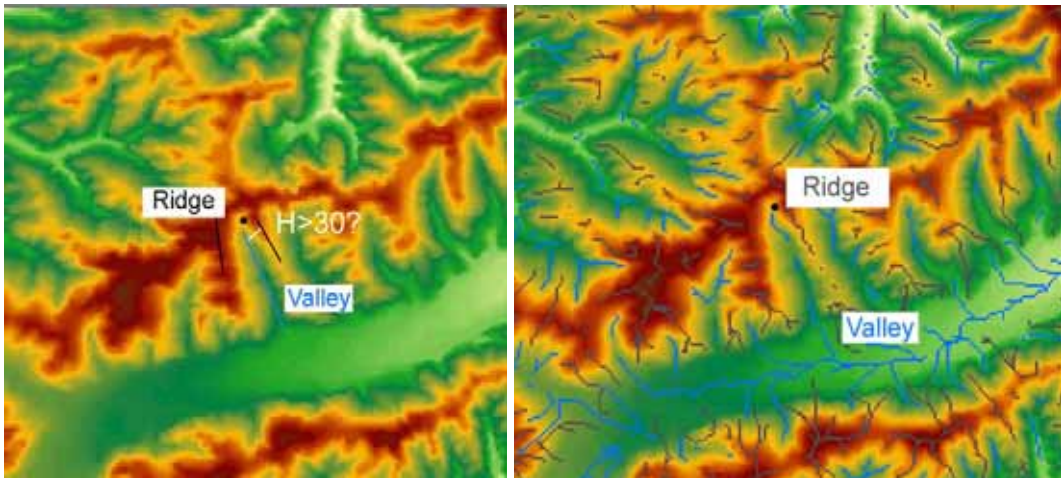

Figure 4.5 Scheme of the ridge –valley identification (left) and resulting GIS analysis (right).

The dot in Figure 4.5 refers to the case of Petritoli (PTI) accelerometric station, that is located at the elevation of 319 m. PTI intersects a ridge feature within a 500 m buffer, and it is placed on a critical slope with $15° < i < 30°$ (see Figure 4.6).

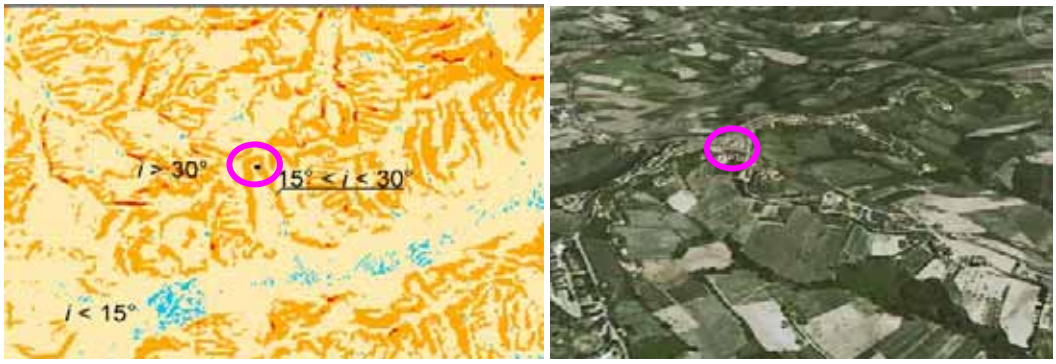

Figure 4.6 Map of critical slope (left) and image of the position of Petritoli (PTI) station (right).

An automatic procedure is still under improvement aimed at the identification of isolated relief than could show larger (> 1.3) amplification factors (Davì, 2008). To clarify the potential amplification of steep topographic irregularities, that cannot be easily reduced to more standard 2D models, 3D numerical analyses have been performed using the spectral element code GeoELSE (http://geoelse.stru.polimi.it/). The resulting degree of amplification can differ from those prescribed for seismic design by EC8 and National codes. The investigation of the correlation between the numerical topographic amplification factors for different morphological configurations with some geometrical parameters such as the aspect ratio (H/L), concavity, bidimensionality index or threshold slope value is presently in progress.

As displayed in Figure 4.7, an automatic GIS procedure has been also proposed to identify isolated topographic irregularities based on the value of the terrain curvature c, that defines valleys as concave areas ($c < 0$) and relieves as convex ones ($c > 0$). By fixing a threshold values c^*, isolated relieves are identified among the convex areas, with $c > c^*$.

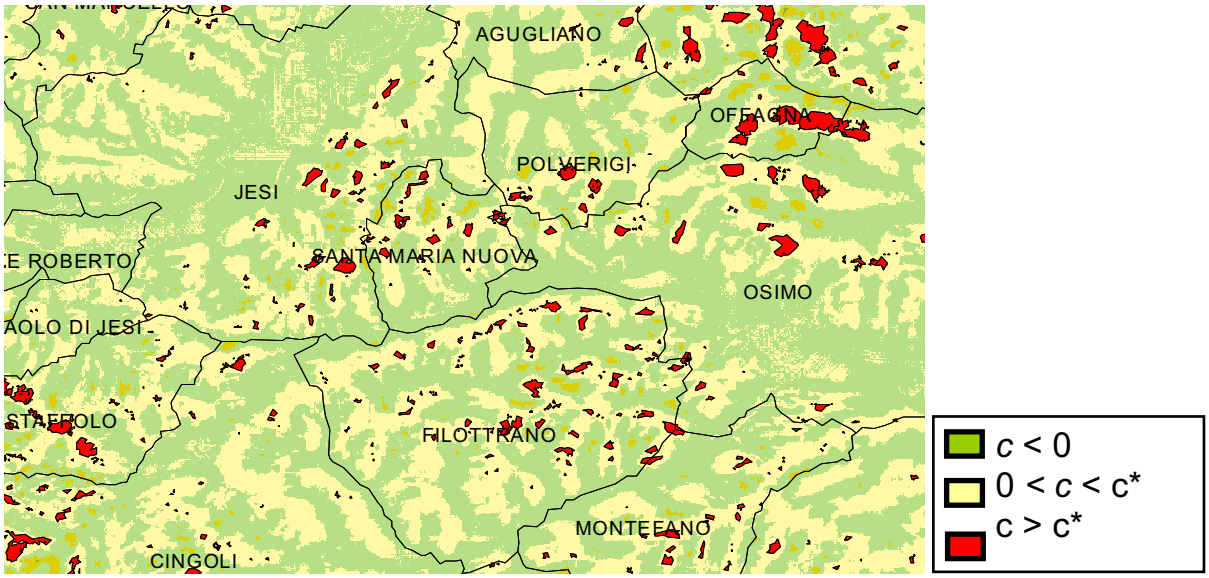

Figure 4.7 Automatic GIS identification of relieves in a territory within Marche region, based on the terrain curvature values. In this case the critical curvature was set to c* = 0.058, empirically calibrated to fit these results with the findings of 3D numerical simulations.

4.4 References

Brambati A, Faccioli E, Carulli EB, Culchi R, Onofri R, Stefanini S, Ulcigrai F. Studio di microzonizzazione sismica dell'area di Tarcento (Friuli) In: Regione Autonoma Friuli-Venezia Giulia and Università degli Studi di Trieste (Eds.), Trieste, 1980.

Davì E. (2008). L'amplificazione del moto sismico indotta d arilievi: simulazioni numeriche 3D, metodi di individuazione e mappatura sul territorio. Master Thesis in Environmental Engineering, Politecnico di Milano.

De Luca G., S. Marcucci, G. Milana, T. Sanò (2005). Evidence of Low-Frequency Amplification in the City of L'Aquila, Central Italy, through a Multidisciplinary Approach Including Strong- and Weak-Motion Data, Ambient Noise, and Numerical Modeling, Bull. Seism. Soc. Am., 95: 1469-1481.

Faccioli E., Vanini M., L Frassine (2002). "Complex" site effects in earthquake round motion, including topography. Proc. 12nd ECEE, London, paper n. 844

Indirizzi e criteri per la microzonazione sismica (2008). Conferenza delle Regioni e delle Province autonome, Presidenza del Consiglio dei Ministri, GdL.

Pacor F., Bindi D., Luzi L., Parolai S., Marzorati S., Monachesi G. (2006). Characteristics of strong ground motion data recorded in the Gubbio sedimentary basin (Central Italy). Bull Earthquake Eng DOI 10.1007/s10518-006-9026-x

Paolucci R. "Amplification of earthquake ground motion by steep topographic irregularities", Earthquake Engineering & Structural Dynamics, Vol. 31, 1831-1853, 2002.

Sirovich L. Southern Italy November 23, 1980 earthquake, Proc. 7th Eur. Conf. on Earthq. Engng., Athens, Greece, 1982; 7: 419-429.

Vanini M., Pessina V., Di Giulio G., Lenti L. (2007) Deliverable D19: influence of alluvium filled basins and edge effects on displacement response spectra, Convenzione INGV - DPC 2004–06, Project S5 – Seismic input in terms of expected spectral displacements

5. Identification of stations with possible soil-structure interaction effects

5.1 Scope

The influence of buildings on free-field ground motion recordings has been postulated for the first time more than 30 years ago (Jennings, 1970; Trifunac, 1975; Wong et al., 1975). In the following years, several papers were devoted to the study of the vibration induced by an impulsive force on real building or on scale models (Kanamori et al.,1991; Erlingsson and Bodare, 1996; Guéguen et al., 2002; Mucciarelli et al., 2003; Gallipoli et al., 2006;) given the difficulty of separating incoming and back-radiated wave field during an earthquake (Chavez-Garcia and Cardenas-Soto, 2002). Some works attempted to use ambient noise to identify the possible fingerprint of buildings in the vicinity of the measurement point (Gallipoli et al., 2004, Cornou et al., 2004, Massa et al. 2009). In the meantime, numerical simulation aimed to reproduce the phenomenon (Bard et al., 1996; Wirgin and Bard,1996;Guéguen et al., 2005; Kham et al., 2006; Ditommaso et al., 2007; Mucciarelli et al., 2008; Ditommaso et al., 2009). In some cases, when an entire town is concerned, numerical simulation were made on idealised models, without a possible comparison with real data (see, e.g., Kham et al., 2006 and references therein). The main disagreement in the literature (Laurenzano et al., 2009) concerns the effects of summations of wave fields from several buildings, which could be constructive or destructive interference. The scope of the research activity reported in this chapter is to identify the presence of the building-soil interaction in the recordings of the ITACA stations. The analyzed stations are listed in Table 5.1.

Table 5.1 List of stations with possible soil-structure interaction effects.

Region	Housing				Number of Records			
	Building (B)	ENEL Box (E_B)	Box	Dam	(B)	(E_B)	Box	Dam
ABRUZZO				VLB				8
BASILICATA	MRV	BRN	STL		7	5	2	
	PTZ	LRG			5	30		
		LRS				14		
CAMPANIA	LVN	ARN	ARI		4	5	5	
		CLT				6		
		MRT				3		
		STR				9		
		TDG				3		
FRIULI	SRCO	BRC	CLA	TLM1	8	4	2	12
		MAI				4		
MARCHE	MNF	CLF	ARQ		6	25	3	
		FHC				4		
		MTL				3		
		PGL				4		
UMBRIA	ASS	BVG	ANNI		76	9	21	
	CLC	CSA			123	9		
	GLT	CSC			8	10		
	NOR	GBP			46	14		
		NCR				46		
		NCR2				136		
		NRC				15		
Number of Stations	9	21	5	2	Total Stations 37			

The analysis technique is rather simple. We took the average of the rotational Horizontal-to-vertical spectral ratios (HVSR) looking for a specific pattern: the signature of the translational modes of a building should be made of two directional peaks (the first higher) separated by 90° (rotational modes make this pattern more complex).
Figure 5.1 reports the behaviour of a pure 1-d amplification effect due to plane-parallel, undisturbed soils (right) and the HVSR atop a 3-storey building (left).

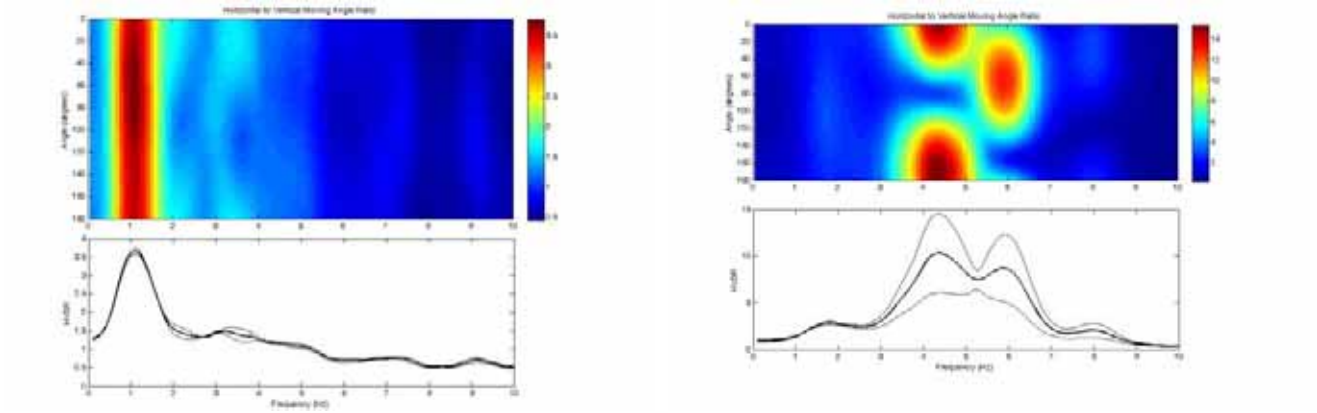

Figure 5.1 Rotational HVSR for 1-d soil (right) and atop a 3-story building (left)

5.2 Stations with possible interaction effects with the hosting structure

We first analysed the effect for station hosted inside a building. The presence of this effect for the station hosted within ENEL sub-station was known since the beginning of the '90s, due to numerical simulation performed at ISMES. Those grey-papers were never published and no field measurement or data analysis were performed to substantiate their findings.
We found that the two-peaks signature is always present within ENEL substations, ranging from 6-8 Hz to 12-18 Hz depending on the building's typology (masonry or pre-cast r.c.).
Figure 5.2 and Figure 5.3 show two representative examples for stations that recorded the Fiuli and Umbria-Marche earthquake respectively.
Also, stations hosted in other buildings may show the presence of peaks due to the structure. This is apparent for the Colfiorito Casermette (CLC), as illustrated in Figure 5.4.

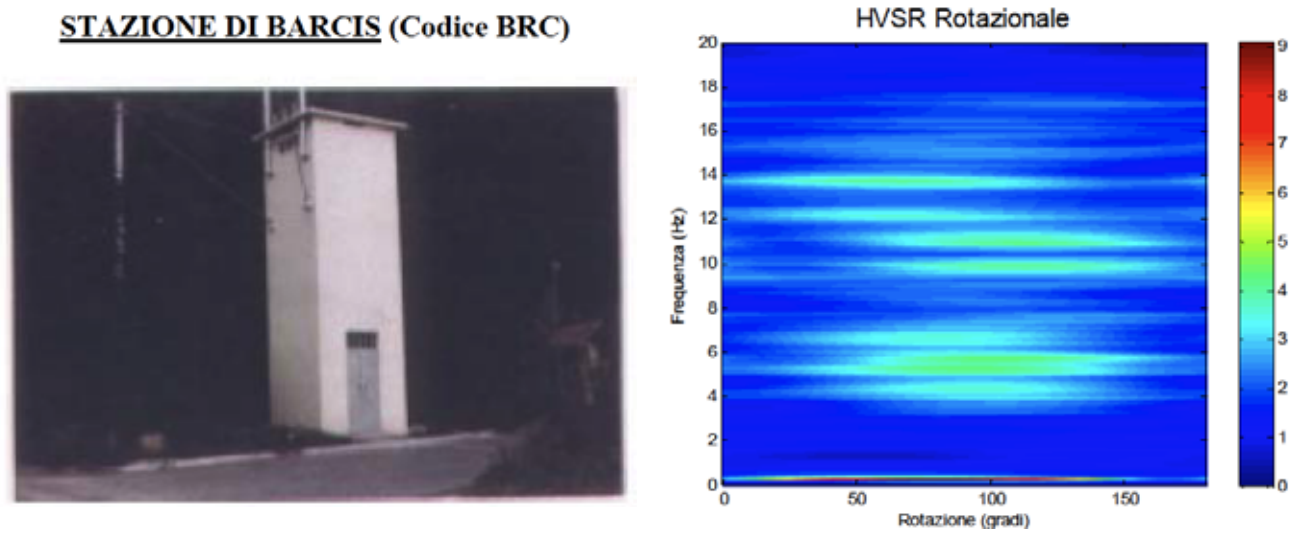

Figure 5.2 Rotational HVSR for the station Barcis in Friuli

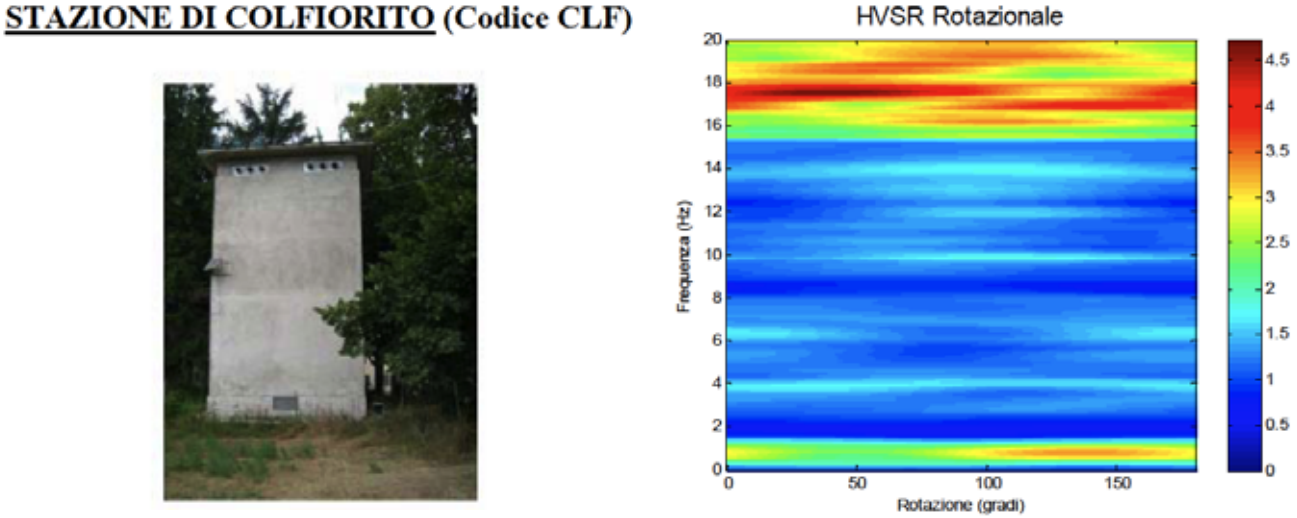

Figure 5.3 Rotational HVSR for the station Colfiorito in Umbria

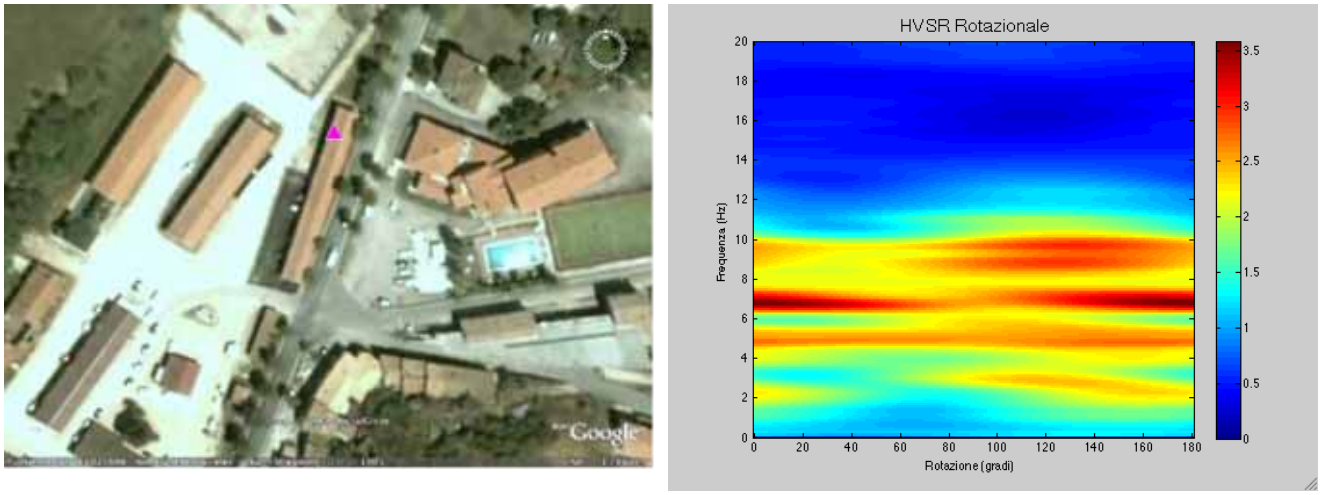

Figure 5.4 Rotational HVSR for the station Colfiorito Casermette in Umbria

5.3 Stations with possible interaction with surrounding buildings and structures

We then considered the interaction with structures located at some distance, starting from dams that are known to affect the recordings as shown for the Italian case of Tolmezzo (Ambiesta Dam) by Barnaba et al. (2007). We observed the structure "footprint" in both the examined cases, the dams at Villetta Barrea and Fiastra (Monte Fiegni station).
Figure 5.5 shows the results for the Villetta Barrea station. Note two peaks at 4 and 6 Hz possibly due to the upstream-downstream motion of the arch dam, and a peak in the E-W direction possibly due to the sloshing of the reservoir. Table 5.2 summarises the preliminary findings of this analysis.

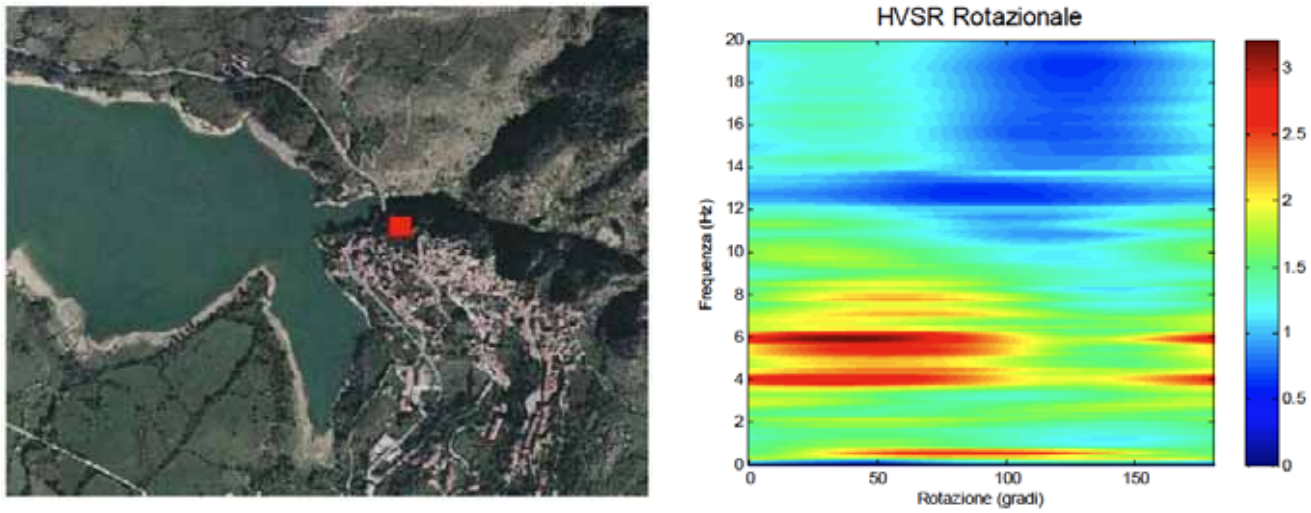

Figure 5.5 Rotational HVSR for the station Villetta Barrea near the same arch dam

Table 5.2 Preliminary findings of the analysis.

REGION	STATION	HOUSING	RECORDS	DIRECTIONAL EFFECTS
FRIULI	Tolmezzo	Dam	12	f = 2Hz, Azimut = N75°
ABRUZZO	Villetta Barrea	Dam	8	f = 4-6Hz, Azimut = N40°
BASILICATA	Marsico Vetere	Building	7	f = 6Hz, Azimut = N75°
	Potenza	Building	5	f = 12Hz, Azimut = N50°
	Brienza	ENEL Box	5	f = 6Hz, Azimut = N75°
	Lauria Galdo	ENEL Box	30	f = 6Hz, Azimut = N75°
	Lauria	ENEL Box	14	f = 10Hz, Azimut = N165°
	Satriano di Lucania	Box	2	f = 4Hz, Azimut = N125° f = 6Hz, Azimut = N160°
CAMPANIA	Laviano	Building	4	f = 2Hz, Azimut = N100°
	Arienzo	ENEL Box	5	f = 5Hz, Azimut = N75°
	Calitri	ENEL Box	6	f = 2Hz, Azimut = N60°
	Mercato S. Severino	ENEL Box	3	no peaks
	Sturno	ENEL Box	9	f = 7Hz, Azimut = N60°
	Torre del Greco	ENEL Box	3	f = 16Hz, Azimut = N20°
	Ariano Irpino	Box	5	f = 1Hz, Azimut = N160°
FRIULI	Forgaria nel Friuli	Building	8	f = 8Hz, Azimut = N90°
	Barcis	ENEL Box	4	f = 5Hz, Azimut = N90°
	Maiano	ENEL Box	4	f = 0.5Hz, Azimut = N140°
	Claut	Box	2	several small peaks
MARCHE	Monte Fiegni	Building	6	several small peaks
	Colfiorito	ENEL Box	25	f = 1Hz, Azimut = N140°
	Forca Canapine	ENEL Box	4	f = 5Hz, Azimut = N75°
	Forca Matelica	ENEL Box	3	f = 20Hz, Azimut = N25°
	Forca Peglio	ENEL Box	4	f = 4Hz, Azimut = N160
	Arquata del Tronto	Box	3	f = 11Hz, Azimut = N125°
UMBRIA	Assisi	Building	76	f = 3Hz, Azimut = N90°
	Colfiorito Casermette	Building	123	f = 3Hz, Azimut = N90°
	Gualdo Tadino	Building	8	f = 18Hz, Azimut = N20°
	Norcia	Building	46	f = 1Hz, Azimut = N125°
	Bevagna	ENEL Box	9	f = 0.5Hz, Azimut = N75°
	Castelnuovo Assisi	ENEL Box	9	f = 3Hz, Azimut = N20°
	Cascia	ENEL Box	10	several peaks
	Gubbio Piana	ENEL Box	14	f = 4Hz, Azimut = N10°
	Nocera Umbra	ENEL Box	46	f = 7Hz, Azimut = N170°
	Nocera Umbra 2	ENEL Box	136	several peaks
	Norcia	ENEL Box	15	f = 6Hz, Azimut = N75°
	Annifo	Box	21	f = 3Hz, Azimut = N160°

5.4 References

Bard, P.-Y., Gueguen, P. and A. Wirgin (1996). A note on the seismic wavefield radiated from large building structures into soft soils, in Proc. of the Eleventh World Conference on Earthquake Engineering, Acapulco, Mexico, Paper No. 1838.

Barnaba, C., Priolo, E., Vuan, A. and Romanelli, M. (2007). Site effect of the Strong-Motion Site at Tolmezzo-Ambiesta Dam in Northeastern Italy, Bull. Seism. Soc. Am., 97, 339-346.

Chavez-Garcia, F.J. and Cardenas-Soto, M. (2002). The contribution of the built environment to the free-field ground motion in Mexico City, Soil Dyn. Earthq. Eng., 22, 773–780.

Cornou, C., Guéguen, P., Bard, P.-Y., and E. Haghshenas (2004). Ambient noise energy bursts observation and modeling: Trapping of harmonic structure-soil induced–waves in a topmost sedimentary layer, J. Seismol., 8(4), 507–524.

Ditommaso, R., Gallipoli, M. R., Mucciarelli, M., Ponzo, F. C. (2007). Effect of vibrating building on “free field” ground motion: from the Bagnoli experiment to many-buildings

simulation. Proc. 4th Int. Conf. Earthq. Geot. Eng.,CD-Rom edition, Paper No. 1388. Springer, ISBN 978-1-4020-5893-6.

Erlingsson S. and Bodare A. (1996) Live load induced vibrations in Ullevi stadium – Dynamic soil analyis; Soil Dyn Earthq. Eng.,15, 171-188.

Gallipoli, M.R., Mucciarelli, M., Castro, R.R., Monachesi, G. and P. Contri (2004). Structure, soilstructure response and effects of damage based on observations of horizontal-to-vertical spectral ratios of microtremors, Soil Dyn. Earthq. Eng., 24, 487-495.

Gallipoli, M. R., M. Mucciarelli, F. Ponzo, M. Dolce, E. D'Alema, M. Maistrello (2006) Buildings as a seismic source: analysis of a release test at Bagnoli, Italy, Bull. Seism. Soc. Am., 96, 2457-2464.

Gueguen, P., Bard, P.-Y. and C.S. Oliveira (2000). Experimental and numerical analysis of soil motion caused by free vibration of a building model, Bull. Seism. Soc. Am., 90, 6, 1464-1479.

Guéguen, P., Bard, P.-Y. and F.J. Chavez-Garcia (2002). Site-city seismic interaction in Mexico Citylike environments: An analytic study, Bull. Seism. Soc. Am., 92, 2, 794- 811.

Gueguen, Ph. and P-Y Bard (2005). Soil-structure and soil-structure-soil interaction: experimental evidence at the Volvi test site, Journ. Earthq. Eng., 9, 5, 657–693.

Jennings P.C. (1970). Distant motion from a building vibration test, Bull. Seism. Soc. Am., 60, 2037-2043.

Kanamori, H., Mori, J., Anderson, D.L., and T.H. Heaton (1991). Seismic excitation by the space shuttle Columbia, Nature, 349, 781–782.

Kham M. J.-F. Semblat, P.-Y. Bard and P. Dangla (2006); Seismic site–city interaction: main governing phenomena through simplified numerical models, Bull. Seism. Soc. Am., 96, 1934-1951.

Laurenzano, G., Priolo, E., Gallipoli, M. R., Mucciarelli, M., Ponzo, F. C. (2009). Effect of vibrating buildings on free-field motion and on adjacent structures: the bonefro (italy) case history, submitted to bull. Seism. Soc. Am.

Mucciarelli, M., Gallipoli, M.R., Ponzo, C.F. and M. Dolce (2003). Seismic waves generated by oscillating building. Soil Dyn. Earthq. Eng., 23, 255-262.

Mucciarelli, M., Ditommaso, R., Gallipoli, M. R. and Ponzo, F. (2008). Effect of Building-Building Interaction on "Free-Field" Ground Motion. Increasing Seismic Safety by Combining Engineering Technologies and Seismological Data. Springer, pp 141-145, ISBN 978-1-4020-9196 -4

Wirgin, A. and P-Y Bard (1996). Effects of building on the duration and amplitude of ground motion in Mexico City, Bull. Seism. Soc. Am., 86, 914-920.

Wong, H.L. and M.D. Trifunac (1975). Two dimensional antiplane building-soil-building interaction for two or more buildings and for incident plane SH waves, Bull. Seismol. Soc. Am., 65, 1863-1865.

6. Monitoring activity

6.1 References

Some of the stations identified as affected by statistically larger amplitudes in Cap.3 have been selected for being investigated in more detail through in-field monitoring activity. These stations are representative of site conditions that are known to favour the increase of ground motion duration and/or amplitude during earthquakes, such as deep basin (Fucino plain), shallow basin (Norcia) and steep topographic relief (Narni). The recording of small magnitude earthquakes at arrays deployed around the selected stations within the duration of the project will help the understanding of physical mechanisms responsible for amplification, a task that cannot be accomplished just using the few available strong motion records of those single stations. The collected data will also provide an experimental basis for numerical modelling.

6.2 Fucino plain

The choice of the Fucino Basin (Central Italy) as one of areas to be monitored in the framework of Task 4 is based both on its geological characteristics and on its importance in terms of seismic risk.
Cavinato et al. (2002) well described the geological and tectonic origin of this basin. "The Basin was the greatest lake of the central Italy, which was completely drained at the end of 19th century. It is an intramontane half-graben filled by Plio–Quaternary alluvial and lacustrine deposits located in the central part of the Apennines chain, which was formed in Upper Pliocene and in Quaternary time by the extensional tectonic activity". The analysis of the geological surface data (Figure 6.1) allows the definition of several stratigraphic units grouped in Lower Units and Upper Units. The Lower Units (Upper Pliocene) are exposed along the northern and north-eastern basin margins. They consist of open to marginal lacustrine deposits, breccia deposits and fluvial deposits. The Upper Units (Lower Pliocene–Holocene) consist of interbedded marginal lacustrine deposits and fluvial deposits; thick coarse-grained fan-delta deposits are interfingered at the foot of the main relief with fluvial–lacustrine deposits. Most of the thickness of the lacustrine sequences (up to 1000 m) is buried below the central part of the Fucino Plain. The basin is bounded by E–W, WSW–ENE and NW–SE fault systems: Velino–Magnola Fault (E–W) and Tremonti–Celano–Aielli Fault (WSW–ENE) and S. Potito–Celano Fault (NW–SE) to the north; the Trasacco Fault, the Pescina–Celano Fault and the Serrone Fault (NW–SE) to the south-east.

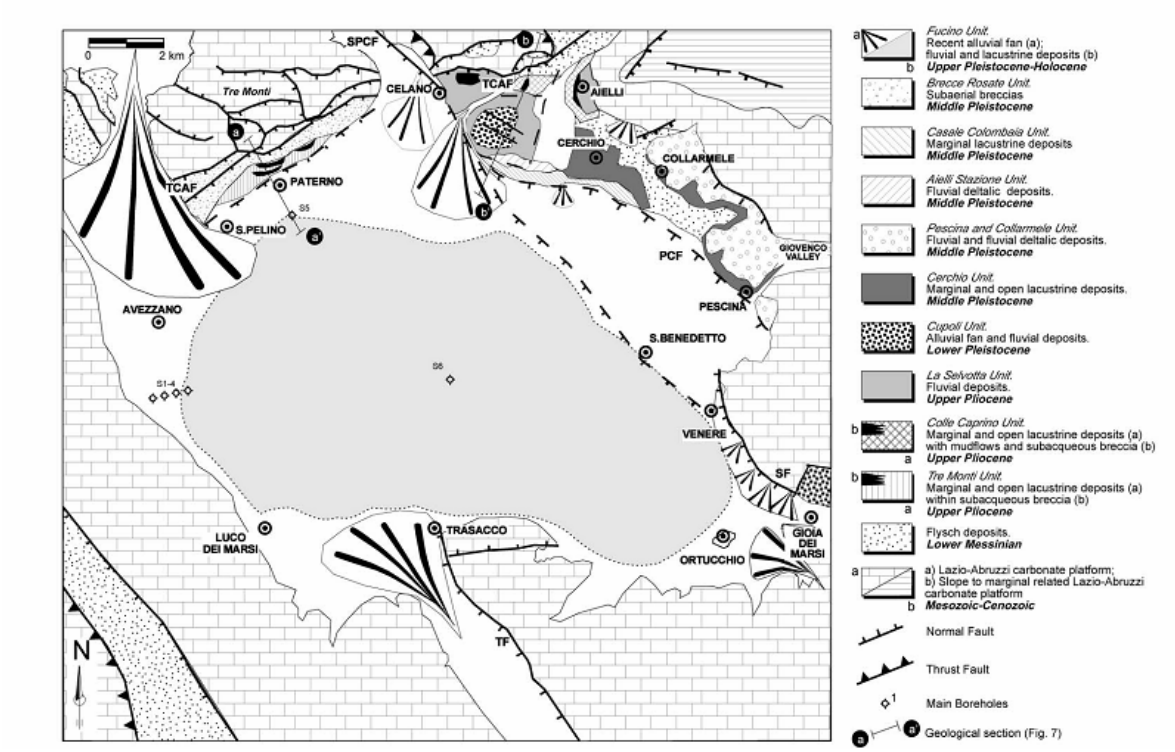

Figure 6.1 Geological map of the Plio–Pleistocene continental deposits, from Cavinato et al. (2002).

The study of industrial seismic profiles across the Fucino Basin gives a clear picture of the subsurface basin geometry; the basin shows triangular-shaped basin-fill geometry, with the maximum deposits thickness toward the main east boundary fault zones. The bottom of the basin is well recognized in the seismic lines available from the good and continuous signals of the top of Meso–Cenozoic carbonate rocks (Cavinato et al., 2002),

The extension of the basin (20 x 15 km) makes it the largest intramontane basin of the central Apennines, the thickness of filling sediments can reach 800-1000 meters as inferred from deep seismic soundings.

From the seismic risk point of view the area suffered in 1915 one of the most severe event in Italian seismic history that caused the complete destruction of many town and villages (including the town of Avezzano) located on the old lake shore. The occurrence of local amplification related to soil characteristics can be reasonably identified as a possible concomitant cause for damage distribution.

The 1915 event fault is located in the eastern edge of the basin and is partially buried by alluvial sediments in the Eastern part of the basin (San Benedetto dei Marsi) area. Except for the major 1915 seismic event the seismicity of the area is quite low and not other important historical events are reported in the Italian catalogues.

Due to its geographic position and to geological characteristics three strong motion instruments of the Italian Strong Motion Network (RAN) were installed in the Fucino Basin starting in 2001. The stations are located in Avezzano (AVZ), Ortucchio (ORC) and Celano (CLN). AVZ is located on Upper Pleistocene – Holocene sediments, while ORC and CLN are installed on rock sites.

The monitoring activity is aimed at detecting amplification effects in different zones of the basin and to relate them to the geometrical and geotechnical properties of the soft sediment layers and to describe the response of the RAN stations operating in the area. The study of the wavefield composition and the detection of potentially dangerous locally generated surface waves is one of the objectives of the activity.

The survey activity started in October 2008 with the objective to find 18 points distributed in the area and located in close and protected sites with available power supply. The network

geometry was selected in order to investigate areas of the basin with inferred variable thickness ranging from less then a hundred meters up to few hundreds of meters. During the site survey phase some preliminary seismic noise measurements were performed to verify the bedrock depth variation along the network through the shift of the resonance frequency peaks found in the HVNSR.

Two main profiles crossing the Basin in the SE-NW and E-W direction were followed during the installation. In the first case (Luco Dei Marsi – Pescina profile) the logistic was quite favorable and it was possible to install 7 stations (LP01 – LP07) along the profile. In the second case (Pescina – Avezzano profile) the lack of both protected places and power supply forced to move northward the designed profile based on 6 stations (PA01 – PA06). Four more sites (PI01 – PI04) were selected to fill up areas not covered by stations. In particular PI01 site corresponds to the station ORC of the RAN and is located on outcropping rocks. One additional rock reference site was deployed NN kilometers away from the basin in the area of the abandoned town of Alba Fucens (RO01).

The first 16 stations were installed during November 2008. In the first stage of the installation one of the instruments was deployed at the RAN sites of AVZ (PA06) located on a sediment site in the eastern part of the basin. The last two stations were deployed in January 2009 to complete the network (Figure 6.2).

The stations are equipped with Lennartz MarsLite or Reftek 130 digital high resolution data loggers. Sensor are the Lennartz LE3d-5s extended band three component seismometers that warranty a frequency response in the 0.2 – 40 Hz frequency band. Stations work in continuous recording with a sample rate of 125 samples per second and synchronized by GPS, data are recorded both on hard drive or compact flash memories with a storage capability of 35 - 40 days.

During the first month of activity the area surrounding the basin was interested by an intense microseismicity, with a seismic swarm which produced a few tenth of events with Ml < 3.0 before April 6, 2009, when the Mw 6.3 L'Aquila earthquake triggered a long sequence of hundreds of aftershocks that have been recorded by the stations.

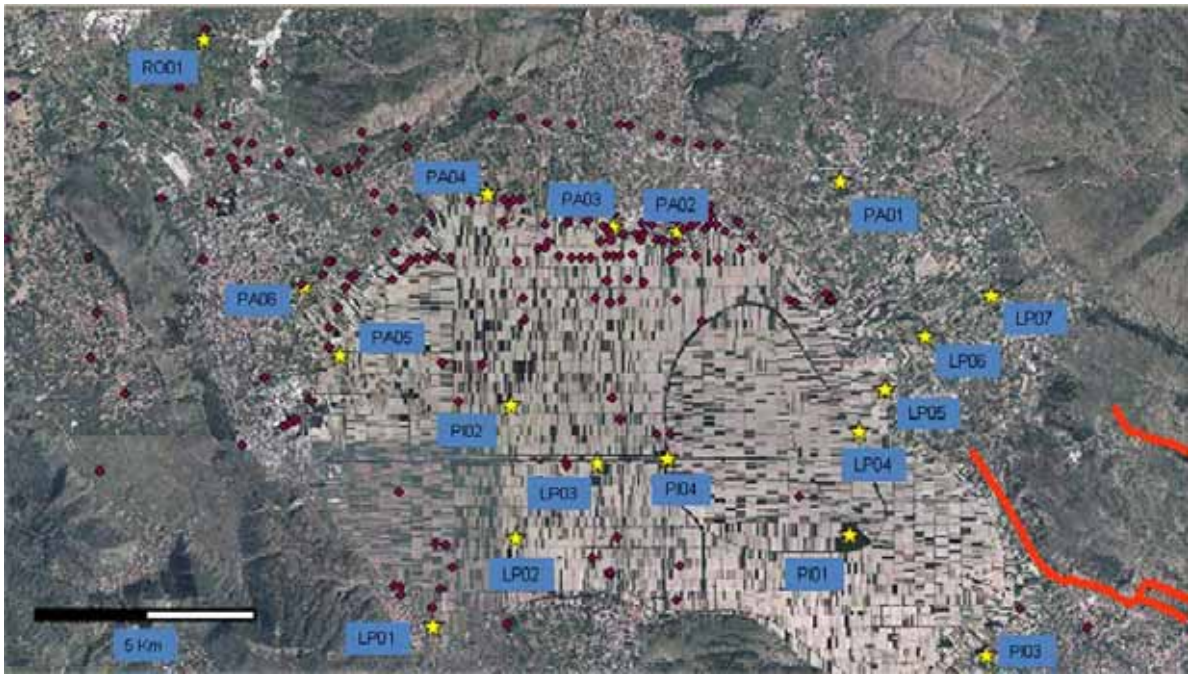

Figure 6.2 Fucino basin temporary network configuration. Yellow stars show the recording stations, red dots indicate deep water wells.

The acquisition of these data is still in progress. A preliminary analysis of data has been performed using two moderate magnitude (Ml 3.5 and 3.6) events happened at about 25-30 kilometers from the basin on February 22 and March 17. The waveforms of these events have been downloaded for all of the 18 stations for the first event and for 17 stations for the second, and show interesting features in the waveforms recorded in the basin.
During the first phase of the monitoring activity data from stations belonging to the INGV national seismic network (RSNC) and from the Abruzzo local network (RCA) were retrieved to construct a complete waveform dataset that includes some other rock site in the area surrounding the basin.

6.3 Norcia

From 17 January 2009 to 24 January 2009 UR8 installed, together with UR1, a seismological network in the area of Norcia. This site was selected as an interesting basin where complicated ground motion amplifications due to 2 or 3D effects can take place. The network is composed by fifteen EarthDataLogger 24 bit acquisition systems equipped with Mark-L-4C-3D short period sensors. The acquisition was set in continuous mode and the sampling rate was fixed to 100 samples per second. The geometry of the network is shown in Figure 6.3. The station position was selected both in order to cover different geological units and to monitor characteristic points for assessing ground motion variability. Logistic problems, like availability of houses and repairs where to install the sensors and to obtain the necessary power supply, also guided the final choice of the sites.

Figure 6.3 Seismological network in Norcia. The red symbols indicate the position of the stations.

Examples of sites where the stations were installed are shown in Figure 6.4 (Station 08 in the southern part of the town) and Figure 6.5 (Station 9 outside the town).
Note that station 09, located on a hard rock site outside of the basin, was installed with a solar panel to guarantee the functioning of the station since a nearby power supply was not available.
UR1 is taking care of the network maintenance with regular inspection of the network every 15-20 days. The network will be de-installed in the week 18-25 of May 2009, and the stations will be used in the following days for performing single station seismic noise measurements and an array.

Figure 6.4 Station 08 located in the southern part of Norcia

Figure 6.5 Station 09 located outside Norcia. The station was equipped with a solar panel due to the lack of nearby power supply.

UR1 released to the project the data set of weak motion recordings collected in Val D'Agri, that has been recognized as a site of particular interest, between September and October 2006. The data started to be analysed in a close cooperation with UR5 with the aim of estimating the site response at the stations of the network. Note that all the 11 stations of the network (Figure 6.6) were equipped with EarthDataLogger 24 bit acquisition systems connected to a Mark-L-4C-3D short period sensor. Stations were set in continuous recording that allowed also an analysis of seismic noise over the whole time of the experiment.

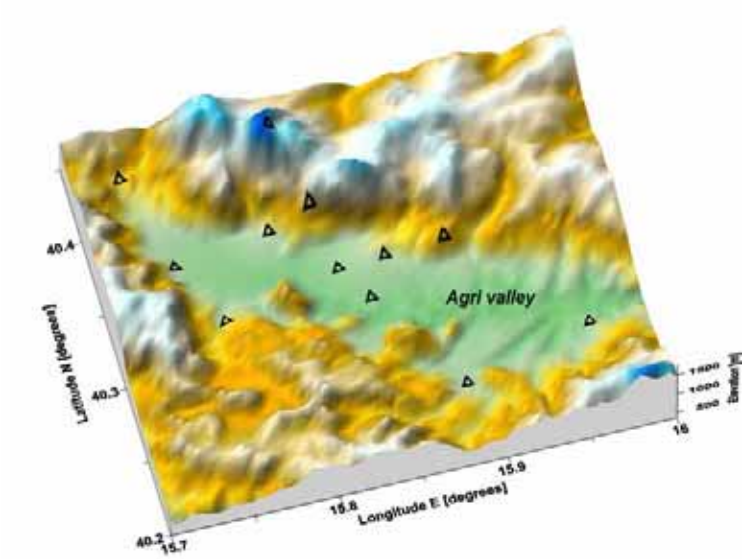

Figure 6.6 The location of the stations in the Agri valley form the seismological experiment carried out between September and October 2006.

Examples of variability during the period of the experiment are shown in Figure 6.7 for one station of the network. The typical daily/weekly cycle due to human activities affecting the noise amplitude at frequency higher than 1 Hz is clearly shown, while low frequency amplitude variations might be related to microseism activity.

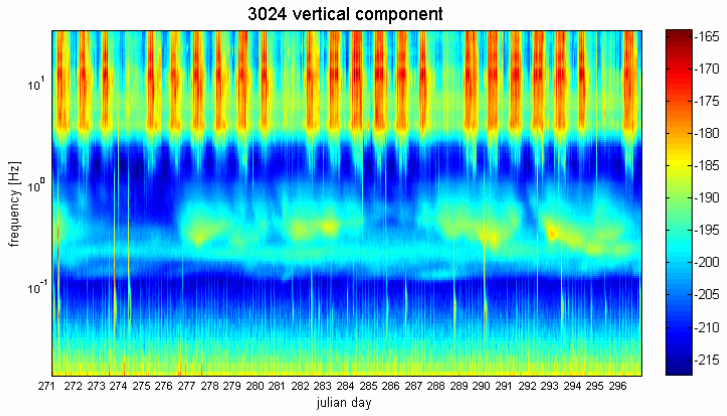

Figure 6.7 Example of power spectral noise density variation versus time.

6.4 Narni

6.4.1 Introduction

The aim of this activity is the monitoring of a topography where an accelerometric station belonging to the National Accelerometric Network (RAN, Rete Accelerometrica Nazionale) was installed.
Narni site was selected after surveying and noise measurements analysis at other two topographies, Montecassino (FR) and Aulla (MS) both having a RAN strong motion station.

The municipality of Narni (TR), in the Umbria region (Central Italy), is expanded on the top of a ridge with NNW-SSE orientation (Figure 6.8) and is characterized by an asimmetry in the steepness with a vertical slope in the SW and NW sides. According to the rules of New Italian

technical rules for building (NTC, 2008), Narni ridge is classified as T3 having a width at the top smaller than width at the base and having a slope between 15° and 30°.
Massive limestone, cherty and marly limestone with very thin marly and clayed levels form the lithology of Narni ridge (Figure 6.8). The level of fracturation of the massive limestone is moderate, especially in the area near the RAN strong motion station NRN so that the geomechanical features do not modify the massive rock. A fracturation associated with strucural elements reported on 1:100000 Geological Map of Italy is particularly evident near the shear zone. This fracturation quickly vanishes away from the mean shear zone becoming meaningless at 10-15 meters from the fault. According to the geomechanical survey, the level of fracturation should not influence the local seismic response. At the base of Narni ridge, alluvial deposits outcrop along the Nera river on west side, while lacustrine and fluvial deposits outcrop on east side locally overlapping, with low angle, the massive limestone. Isolated debris flows are present on southwest and southeast sides.

Figure 6.8 Narni ridge and the RAN strong motion station NRN.

The aim of the study is to evaluate, through an experimental approach, the seismic site response that could affect the recordings at the Narni station, and, more in general, to quantify the amplification factor due to the presence of topographic irregularity, separating the effects due to other effects (for example stratigraphic effects).

On 25 and 26 March 2009 a velocimetric tempory network, for the monitoring of Narni ridge was installed. The seismic network is composed of seven velocimetric stations belonging to INGV-MI-PV (Italian Institute for Geophysics and Volcanology, Department of Milano-Pavia) and CNT (National Earthquake Center). Given the aim of the study the stations were installed at the top of the ridge with a NNW-SSE orientation, in correspondence of east side at the half of the slope and in correspondence of the break of the ridge on west side. Figure 6.9 shows the configuration of the velocimetric network. All stations have been installed directly on rock.

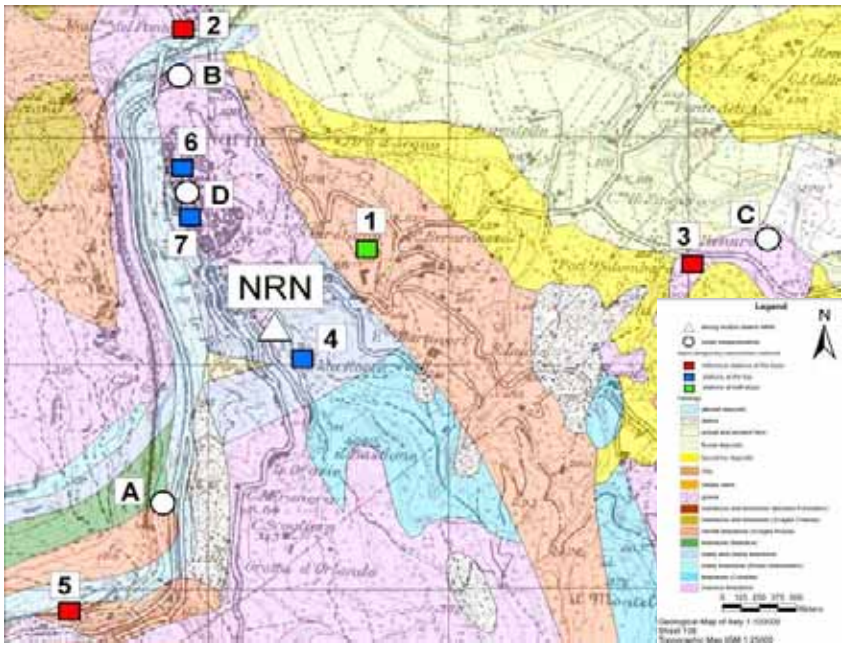

Figure 6.9 Geological map of Narni (from Geological Map of Italy 1:100000) and the temporary velocimetric array: blu, green and red squares show the recording stations respectively at the top, at half slope and at the base of Narni ridge, white dots indicate noise measurements, white triangle indicates the NRN strong motion.

6.4.2 Velocimeter temporary network

The stations used as reference sites were installed at the base of Narni ridge, in the basement of Madonna del Ponte Shrine (NRN2), at ex Miriano aqueduct (NRN3), in free field, and in the court of "Palmira" Restaurant (NRN5). The station at half slope is set on east side in S.Girolamo storehouse theatre and named NRN1. The stations at the top of Narni ridge are NRN4 installed in the basement of Albornaz stronghold, NRN6 in the basement of Narni Civil Protection building and NRN7 in the basement of Eroli Palace in corrispondence of the break of the ridge on west side.

NRN1, NRN3, NRN5, NRN6 and NRN7 stations are provided of Lennartz LE3D-5sec seismometers (flat response in velocity between 0.2 and 40 Hz) equipped with a Reftek 130/01-24 bit data logger. NRN2 and NRN4 stations are provided of Lennartz LE3D-5sec seismometers equipped with MarsLite digital recorders. The sampling ratio is 125 Hz. All stations have electrical connections except for NRN3 stations provided of solar panel. Failing the current, the working is ensured by 12 Volt batteries. Figure 6.10 shows an example of installation at NRN3 station equipped with solar panel.

Figure 6.10 Example of installation of NRN3 station equipped with solar panel.

During the days from 23 to 26 February 2009 ambient noise measurements were performed in different sites of Narni (TR). On the base of the HVSR results, discussed in the following paragraphs, we selected the seven most suitable sites for housing the stations of temporary velocimetric seismic array for the monitoring activity.
The surveyed sites for ambient noise measurements were chosen considering the lithology, the morphology and the logistic. Eleven noise measurements were performed, six of these at the base of Narni ridge, useful to select a good reference site, four at the top and one at east side (Figure 6.9). The selection of reference sites is the most important activity in this phase of work because the differences in site response between the top and the base of the ridge can be explained as due to topographic effects only if the top and the base are under the same conditions.
The noise measurements at the base of Narni ridge were performed on massive limestone and micrite limestone (Scaglia rossa Formation), the ones at the top of Narni ridge were performed on massive limestone and marly and charty limestone and the only one on east side, at the half of the ridge, was performed on micrite limesone (Scaglia rossa Formation).
The ambient seismic noise was recorded for each site using Lennartz LE3D-5sec seismometers (flat response in velocity between 0.2 and 40 Hz) equipped with a Reftek 130/01-24 bit data logger. For each point of measurement at least 30 minutes of ambient seismic noise were recorded at the sampling rate of 100 Hz.
In order to obtain HVSR (Nakamura, 1989), first the mean and the linear trend were removed; a band-pass Butterworth 4 poles filter between 0.2 and 25 Hz was applied. Signals was windowed in time series of 60 s length (cosine taper 5%). For each time window the FFT has been calculated and the power spectral density (PSD) was calculated and then smoothed using the Konno and Ohmachi (1998) window (b=20). HVSRs were computed calculating for each time window the spectral ratio between the root mean square average spectrum of the horizontal components over the vertical ones. At last the average HVSR and the standard deviation have been computed.

The HVSR results from noise measurements do not show differences between the EW and NS components. In Figure 6.11 an example of HVSR results performed at Eroli Palace (NRN7) at the top of Narni ridge.

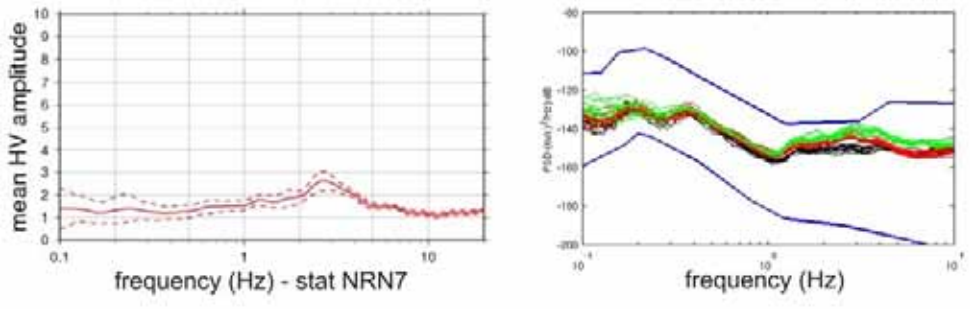

Figure 6.11 Mean NS and EW to Vertical Spectral Ratio and Power Spectral Density.

Sites at the base of Narni ridge (NRNB, NRN2, NRN3, NRNC, NRN5) can be considered reference sites despite a noise background at different frequencies probably due to an anthropic origin. NRNA site (Eon hydroelectric power plant) was the only discarded because of the considerable noise due to the machineries working around the area.
Sites at the top of Narni ridge (NRN, NRN4 and NRN7) exhibit amplification in the frequency range between 2.5 and 3 Hz. It is possible suppose that the peak at 3 Hz could be due to a topographic effect. In attachment *A* HVSR results in detail for all sites.

On 6th April 2009 the seven velocimetric stations of Narni temporary network recorded the Mw 6.3 Aquila earthquake and the following several aftershocks. In Figure 6.12 the non corrected waveforms of NS component recorded at five stations related to Mw 6.3 mainshock and Ml 5.1 aftershock are shown. Table 6.1 shows 16 earthquakes with Ml grater than 4 that the temporary network have been recording since April 6 up to April 23. All earthquakes come from E and SE respect to Narni (NNW-SSE orientation) with azimuth ranging from 114° (Monti della Laga) to 131° (Aquilano) and epicentral distance around 74 Km.

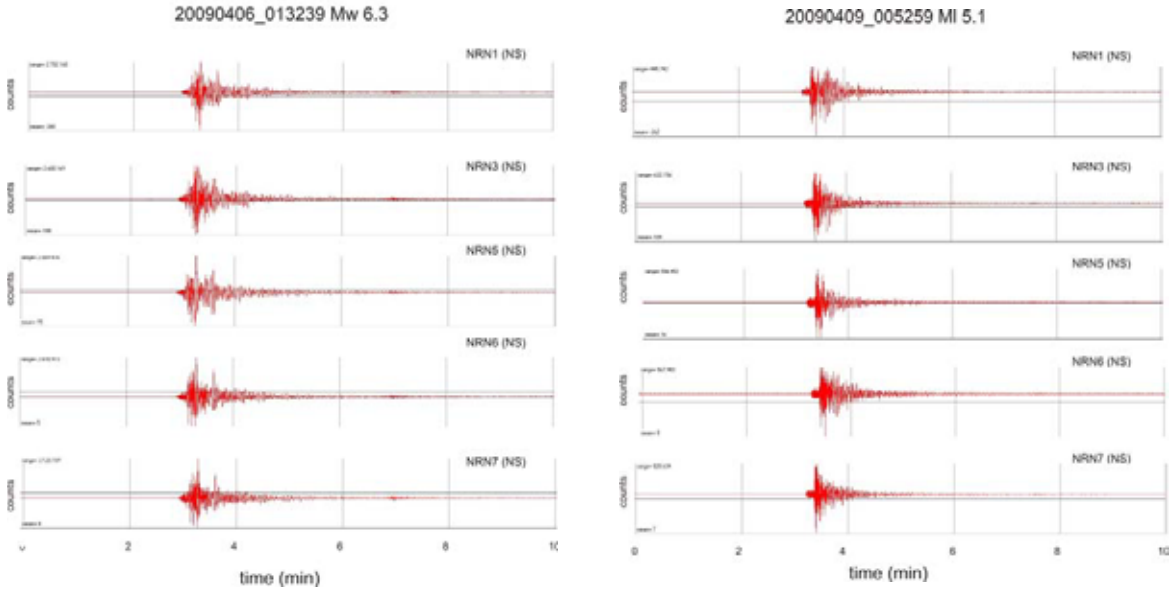

Figure 6.12 NS components of the Mw 6.3 Aquila mainshock and Ml 5.1 aftershock recorded by five Narni stations.

Table 6.1 Earthquakes with Ml grater than 4 recorded by Narni temporary network.

Origin time	Latit.	Long.	Depth (Km)	Magnitude (Ml)	Location	Epi distance (Km)	Azimuth respect

							to Narni
23/04/2009 21:49:00	42.233	13.479	9.3	4.0	Velino Sirente	85	136°
23/04/2009 15:14:08	42.247	13.492	9.9	4.0	Velino Sirente	85	135°
14/04/2009 20:17:27	42.53	13.288	10.4	4.1	Monti della Laga	64	114°
13/04/2009 21:14:24	42.504	13.363	7.5	4.9	Gran Sasso	70	116°
09/04/2009 19:38:16	42.501	13.356	17.2	4.9	Gran Sasso	70	116°
09/04/2009 04:32:44	42.445	13.42	8.1	4.0	Gran Sasso	74	121°
09/04/2009 03:14:52	42.338	13.437	18	4.2	Aquilano	78	129°
09/04/2009 00:52:59	42.484	13.343	15.4	5.1	Gran Sasso	68	118°
08/04/2009 22:56:50	42.507	13.364	10.2	4.3	Gran Sasso	70	115°
07/04/2009 21:34:29	42.38	13.376	7.4	4.2	Aquilano	72	127°
07/04/2009 17:47:37	42.275	13.464	15.1	5.3	Valle dell'Aterno	82	133°
07/04/2009 09:26:28	42.342	13.388	10.2	4.7	Aquilano	74	130°
06/04/2009 23:15:37	42.451	13.364	8.6	4.8	Gran Sasso	70	121°
06/04/2009 16:38:09	42.362	13.333	10.2	4.0	Aquilano	70	129°
06/04/2009 02:37:04	42.366	13.34	10.1	4.6	Aquilano	70	128°
06/04/2009 01:32:39	42.334	13.334	8.8	5.8	Aquilano	70	131°

6.5 References

Cavinato, G.P., Carusi, C., Dall'Asta, M., Miccadei, E. and Piacentini, T. (2002) "Sedimentary and tectonic evolution of Plio–Pleistocene alluvial and lacustrine deposits of Fucino Basin (central Italy)," Sedimentary Geology,148, 29–59.

7. Numerical activity

7.1 Scope

Numerical activity aims at checking the capability of numerical simulations of seismic wave propagation in earth media to reproduce the seismic response of sites characterized by distinctive features induced by complex geological configurations and topographical irregularities. To this end, both the spectral element code GeoELSE (see web site http://geoelse.stru.polimi.it; Stupazzini et al., 2009) and a hybrid Seismic rays-Finite Difference code for seismic wave propagation analyses in 3D heterogeneous media (Orsal et al., 2002) were applied to study the seismic response of the Gubbio plain to the main shock of 1997 Umbria-Marche earthquake sequence (M_W6.0 26.09.1997, time 09.40).
The results illustrated in the sequel clearly point to the need of realistic 3D numerical modelling to predict the combined effects of radiation pattern, propagation path in irregular geological structures and complex site effects, that may be strongly underestimated or neglected at all by numerical approaches based on 1D wave propagation theory.

7.2 3D numerical simulations of the seismic response of Gubbio plain

Numerical analyses in the first part of Project S4 were devoted to the 3D seismic response of the Gubbio sedimentary plain to the main shock of the 1997 Umbria-Marche earthquake sequence (M_W6.0 Sept. 26, 1997, time 09.40). A detailed geological model for the characterization of the seismic response of the Gubbio basin was provided within Project S3 (Deliverable D21) of the previous DPC-INGV agreement.
Leaving to the previous Deliverable and to Pucci et al. (2003) the details about the geomorphology of the Gubbio basin and the seismotectonics context, we limit herein to underline some of its basic features. Gubbio is one of the numerous intramountain basins located in the Central Appennines, a region of extending continental crust within the zone of convergence between the Eurasian and African Plates characterized by mainly SW-dipping and normal-oblique faults (Boncio et al., 2004). It is a 22 km long, 4 km wide sedimentary basin, bounded to the east by the Gubbio Fault, part of the Umbrian fault system (see sketch reproduced in Figure 7.1).
The source parameters are listed in Table 7.1 and were taken from Hernandez et al. (2004). The adopted slip distribution on the fault plane is depicted in Figure 7.2a, while the time dependency of the seismic moment tensor source is illustrated in Figure 7.2b.
As a reasonable approximation, a simplified homogenous description of the dynamic properties of the Gubbio plain was assumed, based on the following polynomial variation with depth z (measured in m):

$$V_P = 1000+30\, z^{1/2},\ V_S = 250+19 z^{1/2},\ \rho = 1900 \text{ and } Q_S = 50 \qquad (7.1)$$

where V_P and V_S are the P- and S- wave velocity (in m/s), respectively, ρ is the mass density (in kg/m^3), and Q_S is the S- wave quality factor. The linear gradient for V_P and V_S of Eq. (7.1) was calibrated to represent an ideal "average" soil profile in the Gubbio valley based on the V_S profiles available from Project S3 DPC-INGV (Deliverable D21), as reported in Figure 7.3.
The crustal velocity model is layered and described in Table 7.2. It combines the results from the geological investigation performed in the previous Project S3 with the description given by Hernandez et al. (2004) and by Mirabella et al. (2004).

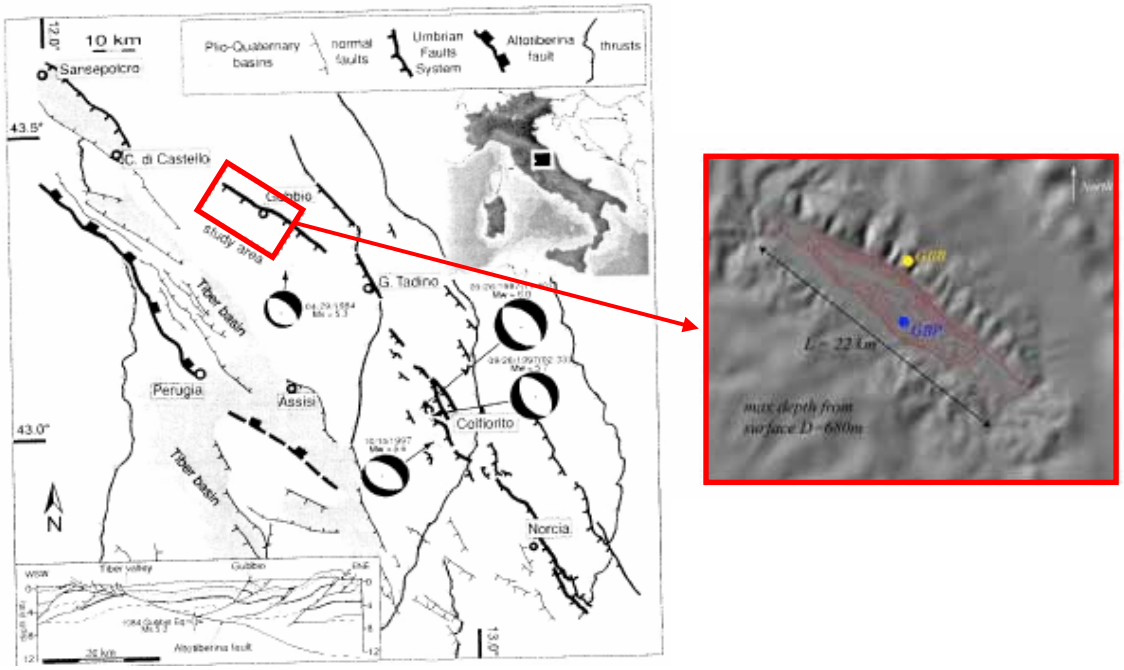

Figure 7.1 Left: sketch of the Umbria fault system highlighting the location of the investigated area (superimposed box). From Pucci et al. (2003). Right: detail of the Gubbio basin, the position of the GBB (Gubbio downtown) and GBP (Gubbio plain) accelerometric strong motion stations is also indicated (filled dots).

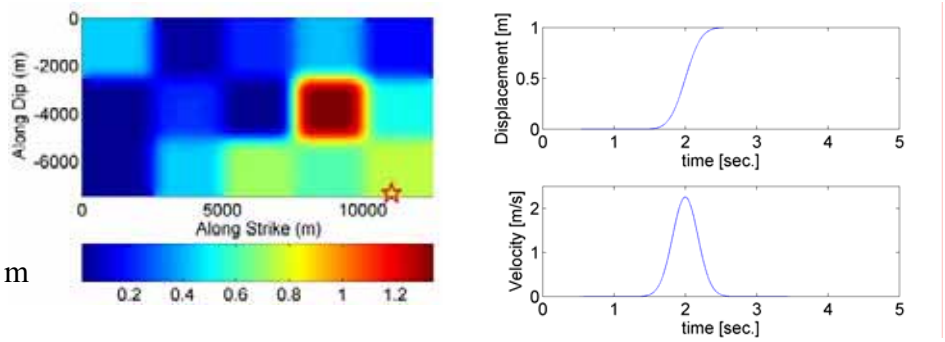

Figure 7.2 Left: slip distribution for the M_w6 Colfiorito #2 event 26.09.97 (9:40). (Model M7 of Hernandez et al., 2004; available at the web-site http://www.seismo.ethz.ch/srcmod). Right: source time function for the simulated earthquake (see Table 7.1).

Table 7.1 Source parameters used for the Umbria-Marche event 26.09.1997 (9:40, M_W = 6.0). (from Hernandez et al., 2004).

HYPOCENTER [°N,°E,Z]	*M_0 [N m]*	*L x W* [km]	Strike [deg]	Dip [deg]	Rake [deg]	*Depth of upper points [km]*	*Vr* [km/s]	rise time τ [s]
43.0255°N, 12.8917°E 5700 m depth	$8.1 \cdot 10^{17}$	12.5 x 7.5	144	42	270	0.7	2.6	1

Table 7.2 Layered crustal model: layers are listed from top (ground surface) to bottom.

Layer #	H (m)	V_P [m/s]	V_S [m/s]	ρ [kg/m^3]	Q_S
B1	1100	3500	1800	2200	80
B2	1586	4000	2200	2400	100
B3	1000	4800	2666	2600	150
B4	3000	5500	3055	2800	250
B5	-	6300	3500	2900	300

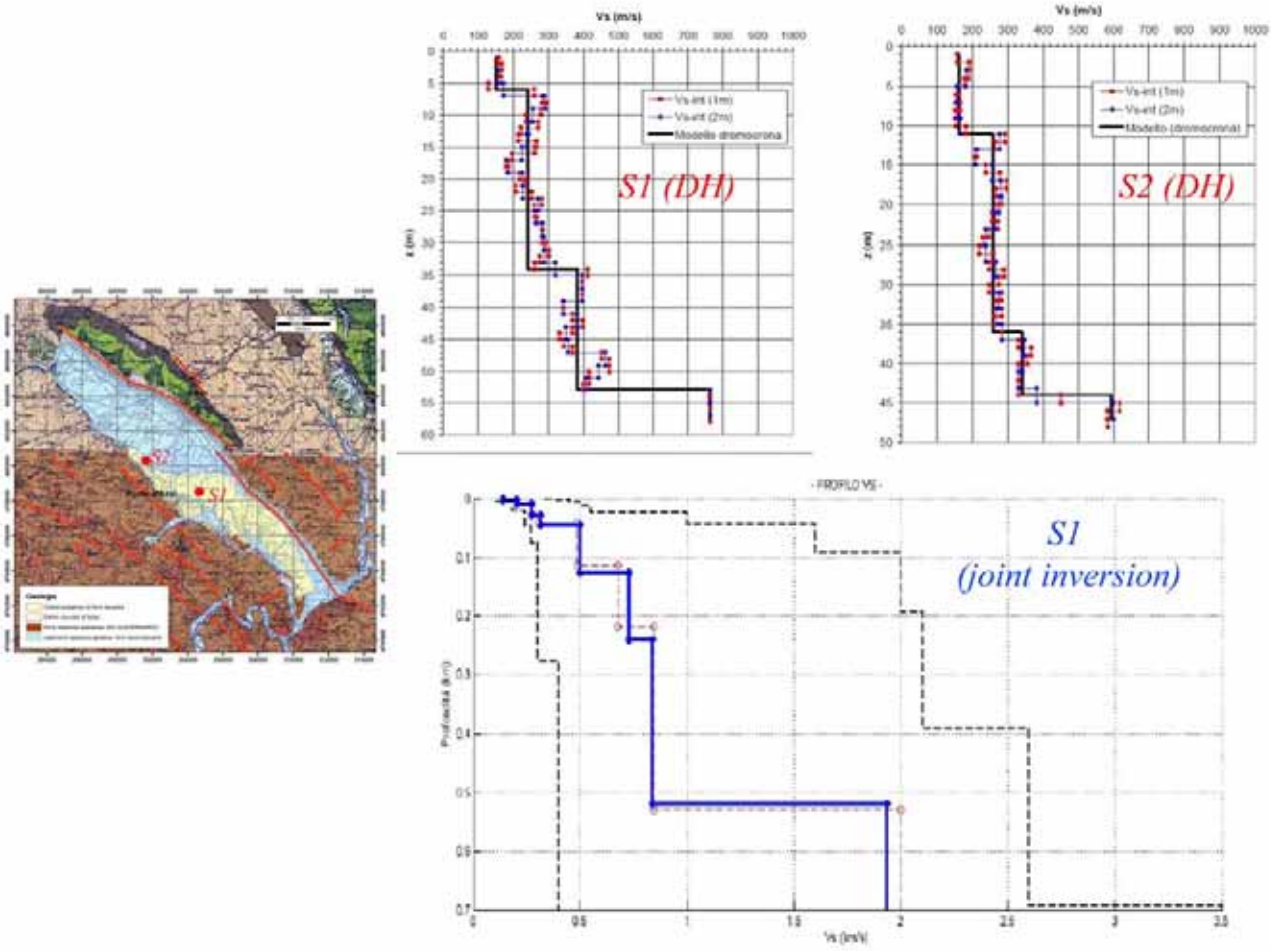

Figure 7.3 V_S and V_P profiles from downhole (DH) measurements and from joint inversion of dispersion and H/V curves at sites S1 and S2 (see map on the left-hand-side). From Project S3 DPC-INGV (Deliverable D21).

7.3 3D large-scale modelling by means of a Spectral Element Code (GeoElse)

7.3.1 Spatial Discretization

The 3D spatial discretization of the Gubbio basin and its surrounding requires to build up a large unstructured mesh of hexahedral spectral elements. While the construction of such a mesh using tetrahedral elements can be easily achieved by commercial or non commercial software, creating a complex hexahedral mesh is still a challenging problem since most of hex meshing algorithms currently in use are limited in scope, i.e., they only apply to a subset of geometries. In this work, we successfully mesh the computational domain thanks to the software CUBIT (http://cubit.sandia.gov/), which incorporates a set of powerful and advanced meshing schemes specifically developed to handle the hexahedral unstructured meshing problem. A thorough description of the meshing strategy adopted to strictly honor the geometry of the Grenoble basin can be found in Stupazzini et al. (2009).
The mesh of Gubbio was designed thanks to the so called “Not Honoring” (NH) technique. This can be described as a "three steps" procedure: the starting point is a coarse mesh (1000 m size) with element honoring only the topographical constrain. The deep geometry of the alluvial basin is given as a "soft" constrain: the green volume in Figure 7.4 includes the alluvial basin solid and has a simplified geometrical shape compared to the real shape of the alluvial basin. It is worth to note that 1000 m is a size of the element compatible with a

correct sampling of a peak frequency f_{max} = 2Hz, propagating inside the outcropping bedrock (V_S = 1800 m/s). The strategy basically drives the element size from 1000 m down to 100 m, and this size is compatible with a correct sampling up to 3 Hz of the upper part of the alluvial deposit (Vs = 300 m/s) with a SD equal to 4. This procedure can be programmed into script and can be parallelized.
The final mesh obtained with the "three steps" strategy is presented in Figure 7.4a: the domain is fully unstructured and for simplicity only the spectral elements are shown without GLL nodes. The inner volume (green color), where the second level of refinement takes place (Figure 7.4b, up and bottom) is extracted from the mesh to better highlight the internal design and the 3D unstructured mesh. To efficiently assign the mechanical properties of the basin, a specific description of the alluvium-bedrock interface by a triangular decomposition is introduced, as shown in Figure 7.5, so that each nodal point of the mesh is automatically associated to the corresponding soil material.
The final mesh consists of 361,752 elements, the size of which ranges from a minimum of about 100 m (inside the alluvial basin) up to 900 m. The mesh is designed to propagate frequencies up to around 3 Hz with spectral degree SD = 4. The numerical simulations were performed with both the Tethys (Oeser et al., 2006) and the Lagrange (www.supercomputing.it) parallel computer clusters. The main characteristics and the performance of the numerical analyses, referring for simplicity to the Lagrange cluster alone, are summarized in Table 7.3.

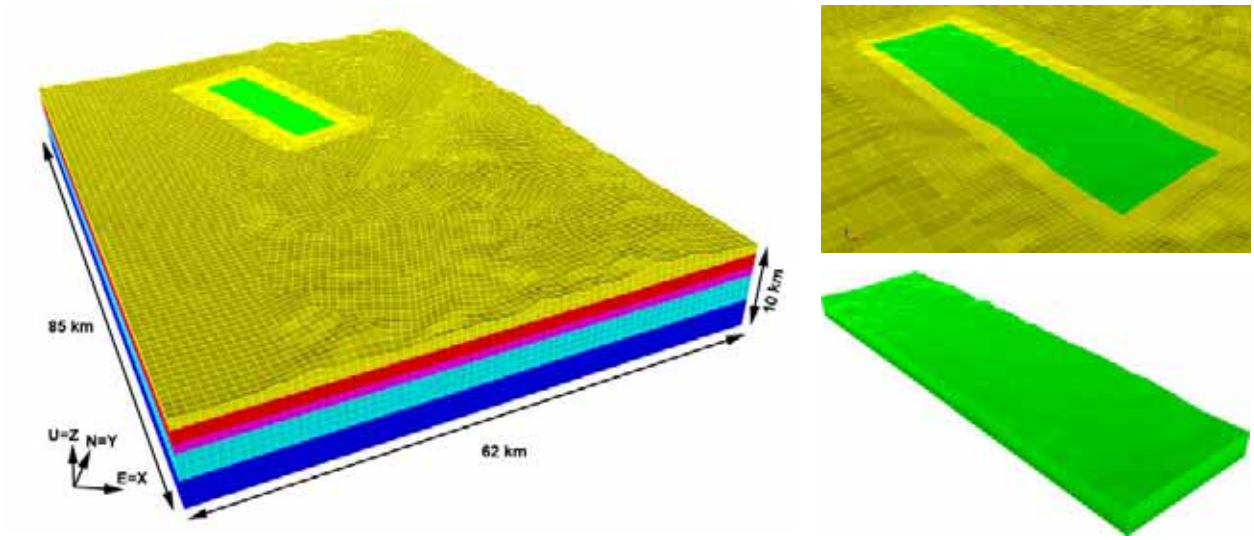

a) **b)**

Figure 7.4 (a) 3D hexahedral spectral element mesh adopted for the computation of the Gubbio case study, with the GeoELSE software package. The computational domain is subdivided into small chunks, each of them is sequentially meshed starting from the alluvial basin down to the bedrock. For simplicity, the spectral elements are shown without the LGL nodes. b) Detailed view of the Gubbio mesh in the surroundings of the alluvial basin mesh.

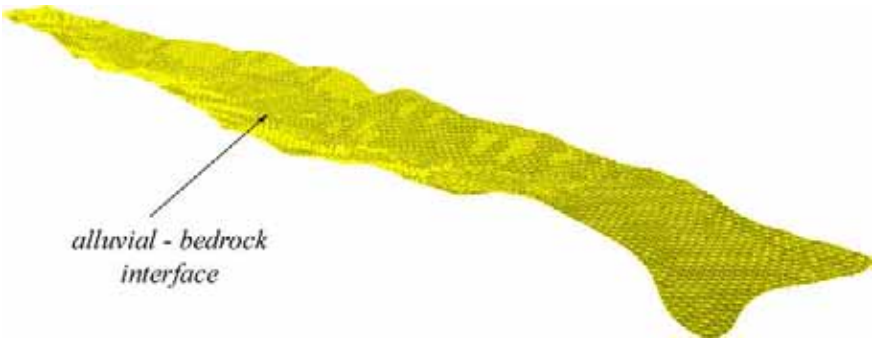

Figure 7.5 Triangular decomposition of the interface between the alluvial deposits and bedrock.

Table 7.3 3D numerical model size and computational time. Data of CPU time refer to the Lagrange cluster (www.supercomputing.it).

SD	Elements #	Nodes #	$\Delta t_{simulation}$ [sec.]	$\underline{\Delta t}_{CFL}$ [sec.]	Total simulated time [s.]	Total CPU time (48 CPUs) [min]	Set-up time [sec.]
4	361,752	2,3498,665	$3.4483 \cdot 10^{-4}$	$1.831 \cdot 10^{-3}$	100	8,962 (~149.4 hours)	8640 (~144 min)

7.3.2 Results

Figure 7.6a and Figure 7.6b illustrate, respectively, the Peak Ground Displacement, PGD, and Peak Ground Velocity, PGV, calculated as the geometric mean of the horizontal components, for a set of receivers located in the Gubbio plain (left) and on outcropping bedrock (right). The numerical values (filled dots) are in good agreement with estimates given by the EGMPEs proposed by Cauzzi & Faccioli (2008), for PGD (specifically, spectral displacement ordinate at T=20s), and by Akkar & Bommer (2007), for PGV. It is interesting to note that the values corresponding to station GBP (Gubbio piana, see superimposed dots on the graphs in the left panel) are systematically above the 84° percentile of the EGMPEs, confirming the occurrence of significant ground motion amplifications at long periods. In Figure 7.7 and Figure 7.8 the simulated velocity and displacement time histories at GBP are compared with the recorded ones along with the corresponding Fourier spectra. The same comparison is illustrated in Figure 7.9 and Figure 7.10 for station GBB (Gubbio), lying on an alluvial terrace at the edge of the basin. Synthetics and observations are filtered with an acausal Butterworth filter with high pass frequency f_h=0.1 Hz, for GBP, and f_h=0.4 Hz, for GBB and low pass frequency f_l=3 Hz in both cases.

The previous comparisons show that the accuracy achieved by 3D numerical simulations to predict the observed ground motions in the range of frequencies below 3 Hz is remarkable, when we consider that the input just consists of the kinematic seismic source model by Hernandez et al. (2004) and only a relatively rough approximation of the crustal model and of the Gubbio basin model is available.

To clarify the power of such advanced numerical simulations with standard approaches for earthquake ground motion predictions, we plot first in Figure 7.11 the 5% damped acceleration response spectra obtained by the numerical simulations at GBP and GBB (red line) compared with the recorded ones (black) and with the predictions of several EGMPEs. In agreement with observations, the 3D approach predicts at GBP (left side) the observed exceedence of the 84° percentile of the EGMPEs for all periods beyond about 0.6 s. On the other hand, where the basin effect is negligible such as at GBB, the predictions by EGMPEs

are satisfactory. In both GBP and GBB cases, the underestimation of the numerical simulations at short periods, below about 0.3 s, is due to the frequency limitation of the numerical model.

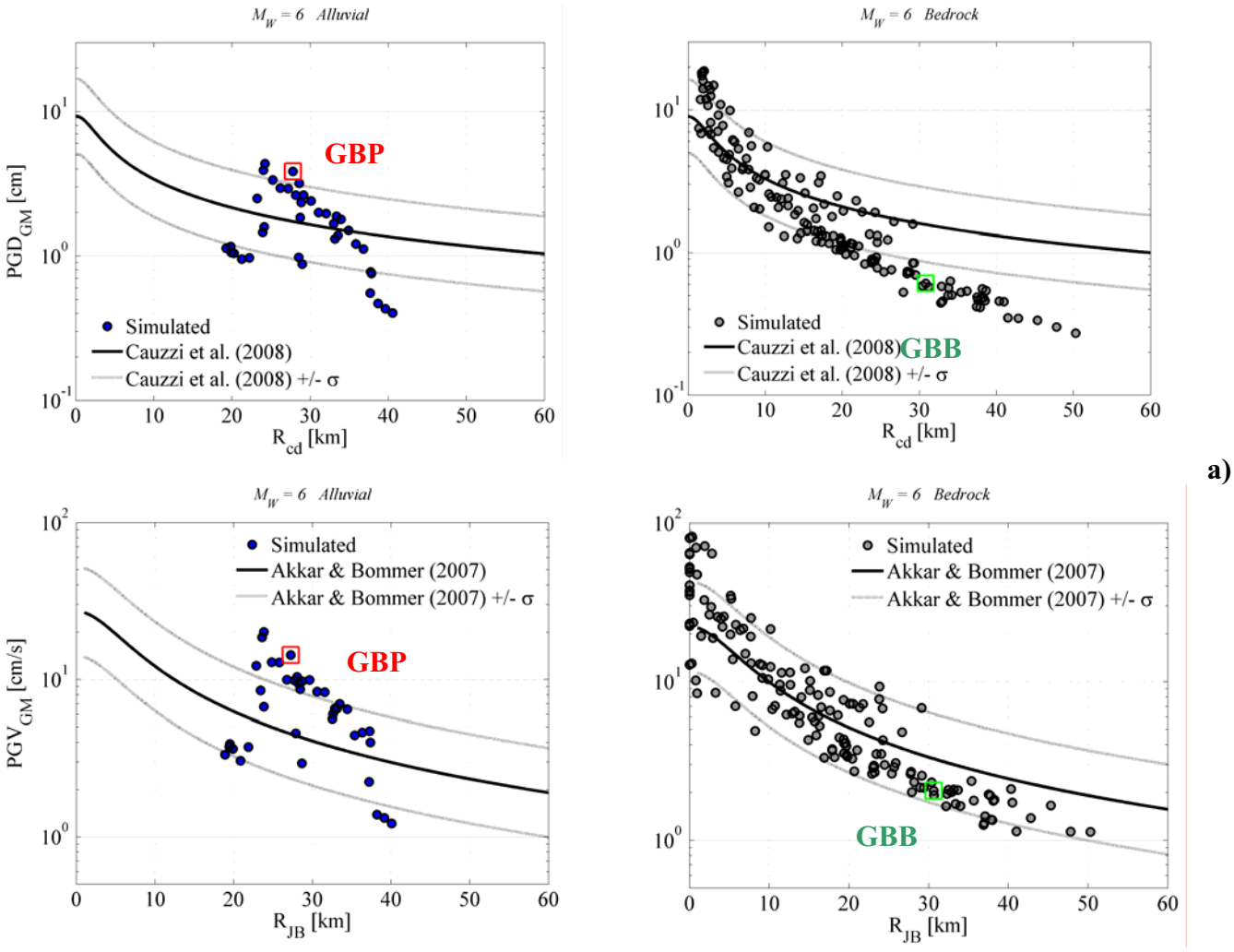

Figure 7.6 a) comparison of the Peak Ground Displacement PGD (geometric mean) values obtained by means of 3D numerical simulations (filled dot) with the predictions from Cauzzi & Faccioli (2008) for a set of receivers in the alluvial basin (left) and on bedrock (right). b) as in a) but in terms of Peak Ground Velocity (PGV, geometric mean) values: comparison with the ground motion model proposed by Akkar & Bommer (2007). The small boxes denote the receivers corresponding to GBP and GBB stations.

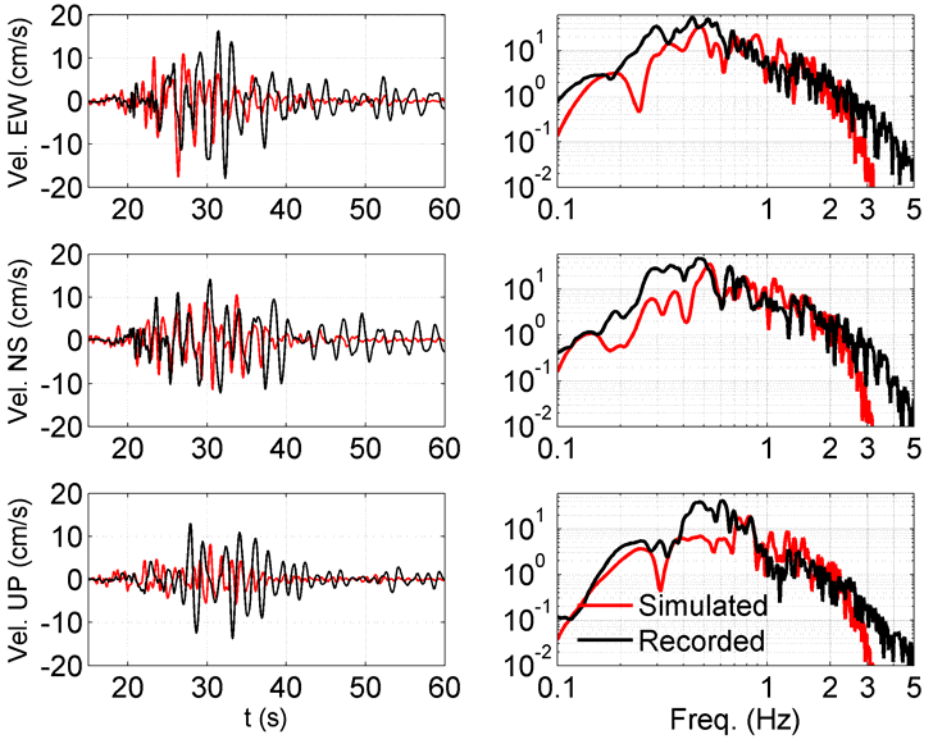

Figure 7.7 3D numerical simulation vs. observation: velocity time histories (left) and corresponding Fourier amplitude spectra (right) obtained at station GBP (Gubbio Piana).

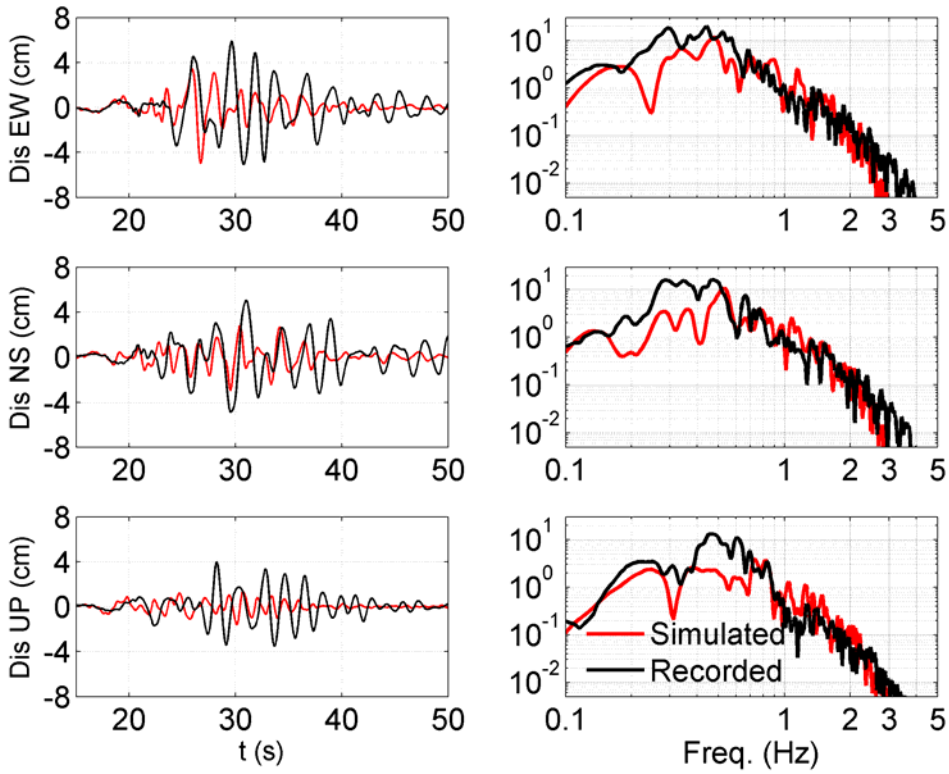

Figure 7.8 As in Figure 7.7 but in terms of displacement.

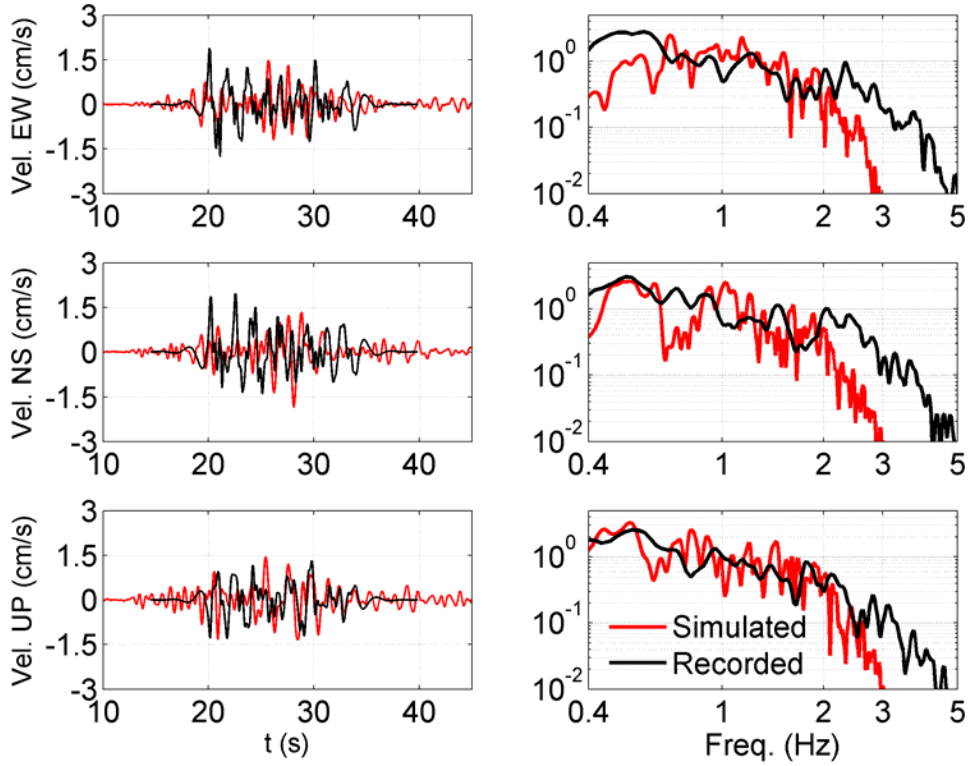

Figure 7.9 3D numerical simulation vs. observation: velocity time histories (left) and corresponding Fourier amplitude spectra (right) obtained at station GBB (Gubbio downtown).

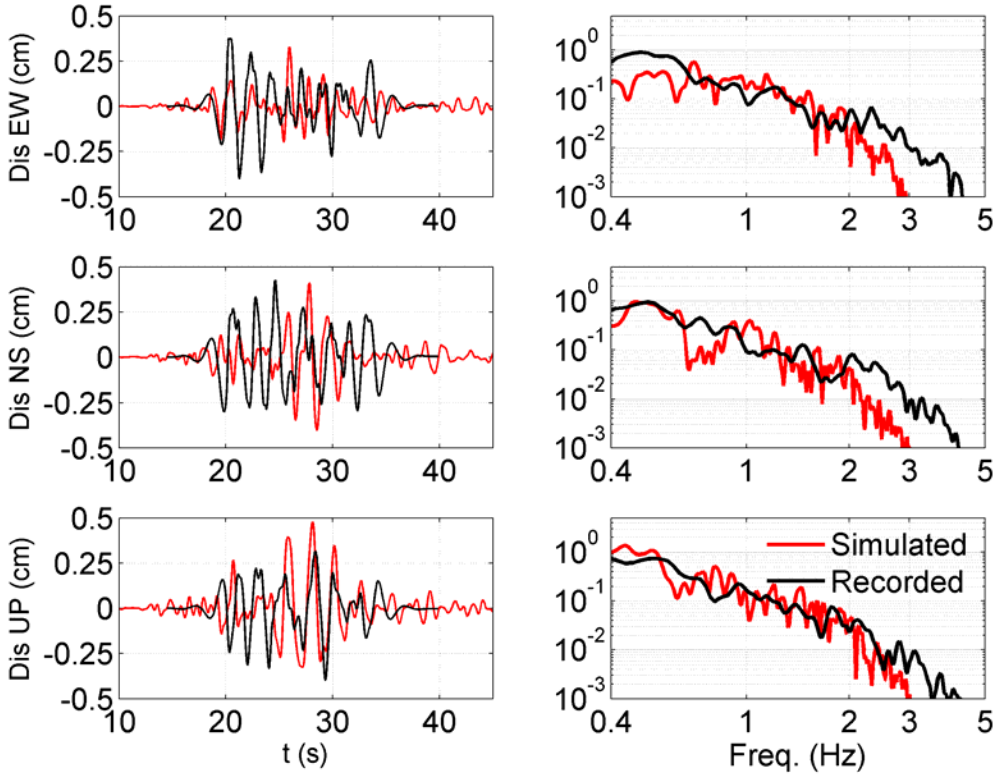

Figure 7.10 As in Figure 7.9 but in terms of displacement.

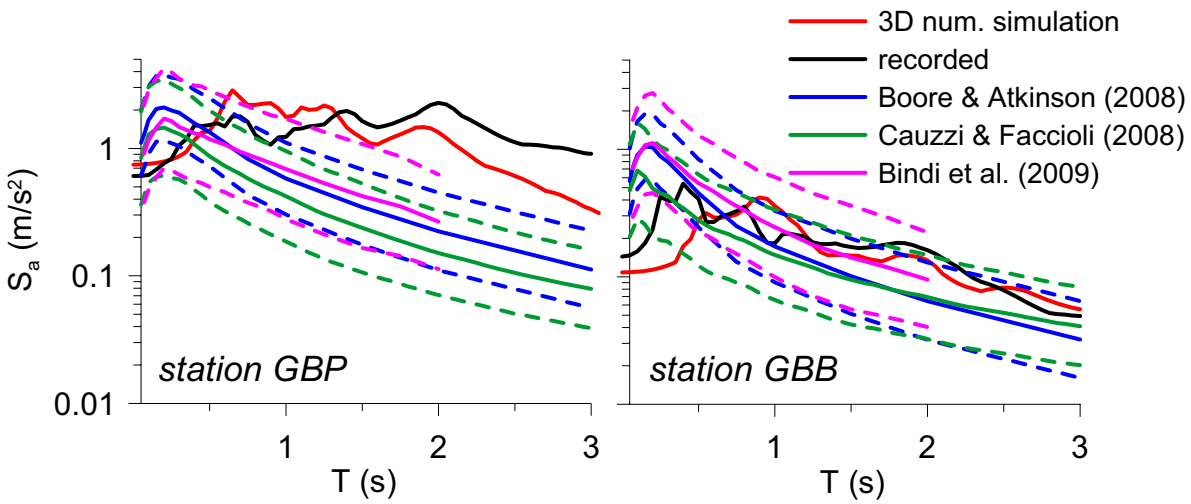

Figure 7.11 Acceleration response spectra at 5% damping at GBP (a) and GBB (b): comparison of the numerical simulation (red line) with the recordings (black line) and the spectral ordinates as predicted by Boore & Atkinson (2008), Cauzzi & Faccioli (2008) and Bindi et al. (2009).

Secondly, Figure 7.12 shows the comparison between the observed and 3D simulated Fourier spectral ratios at GBP with respect to the nearby reference rock station GBB (see location in Figure 7.1) for the M_W6.0 event 26.09.1997 9.40. Furthermore, the analytical 1D transfer functions, computed assuming under GBP both the soil profile of Eq. (7.1) and of Table 7.4 (obtained from the available data), are also displayed for comparison. It is apparent that the long period basin-induced amplification observed at GBP cannot be predicted by the 1D model. Instead, the agreement with the numerical 3D spectral ratio for T>~1 s is remarkable, and clearly points out that the distinctive features of long period ground response in the presence of a deep closed-shape sedimentary basin such as Gubbio cannot be accurately predicted but with advanced numerical tools based on 3D wave propagation theory.

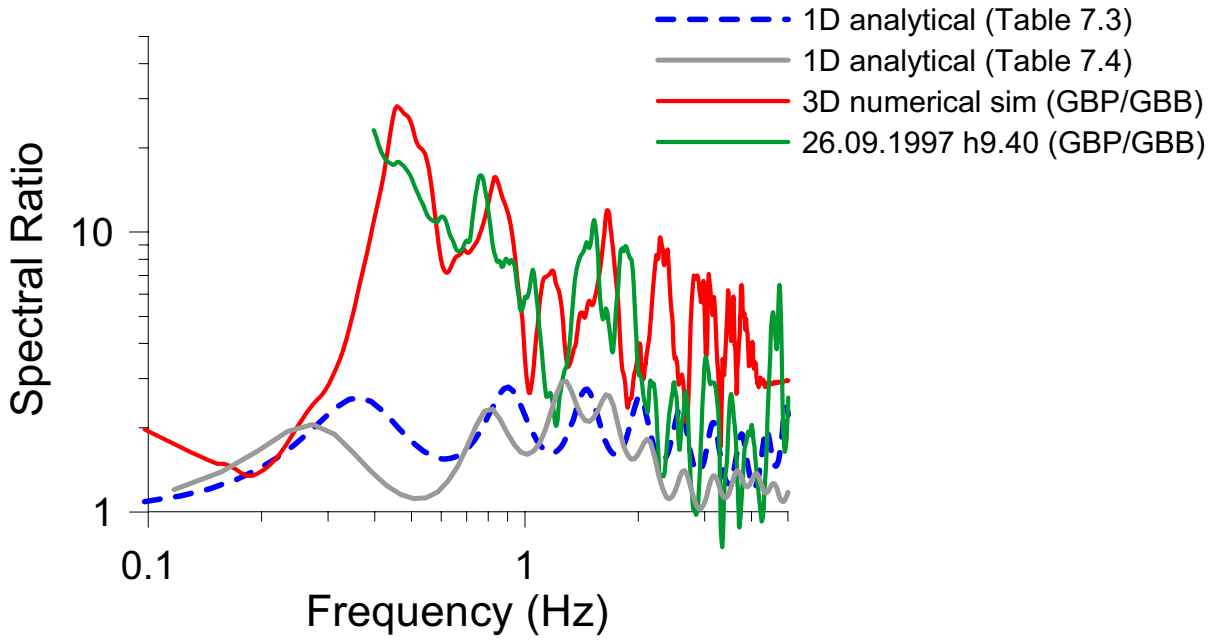

Figure 7.12 Comparison between observed and simulated spectral ratio of GBP with respect to the nearby reference rock station GBB. The analytical 1D transfer function, obtained assuming the parabolic distribution of *Vs* with *z* as in Eq. (7.1) is also superimposed.

Table 7.4 Layered soil profile under GBP used for computing 1D model adopted for the Gubbio plain.

Layer	H [m]	V_S [m/s]	ρ [kg/m^3]	Q_S
A1	5	151	1750	10
A2	29	240	1850	10
A3	21	383	1850	10
A4	500	600	2000	20
A5	-	1200	2150	100

7.4 Preliminary numerical results by means of a hybrid Ray-Finite Difference code

Additionally to the use of the spectral element code GeoELSE and for checking the capability of the results, numerical simulations based on a 3D hybrid ray-finite differences code were carried out using the parameters of the 1997 Umbria-Marche earthquake sequence (M_W6.0 26.09.1997, time 09.40, see Table 7.1).
This two step approach is based on the decomposition of the numerical model in two parts: the external domain, including the seismic source and a simplified 1D crustal structure, which is solved by the seismic ray theory, while the inner domain includes the complex geological structure where the calculations are carried out by finite difference (FD) numerical techniques. (see Oprsâl et al. 2002 for further details).
A numerical FD model of the Gubbio basin was setup, to propagate the wavefield up to 6 Hz, with the same seismic source, basin shape and dynamic properties as described previously. Several simulations have been carried out to verify the influence on seismic wave propagation of different material parameters (Table 7.2 and Eq. (7.1)). Snapshots of the simulated peak ground displacements illustrate that significant amplification occurs inside the basin, with clear diffraction of the wavefield at the edge of the basin and wave propagation towards its center (Figure 7.13).
Comparison between results obtained by this hybrid approach and the observations is in progress. Preliminary results show a satisfactory agreement in terms of peak ground displacement, velocity and duration (Figure 7.14). As noted previously, a similar agreement could not be obtained by standard 1D plane wave propagation approaches.

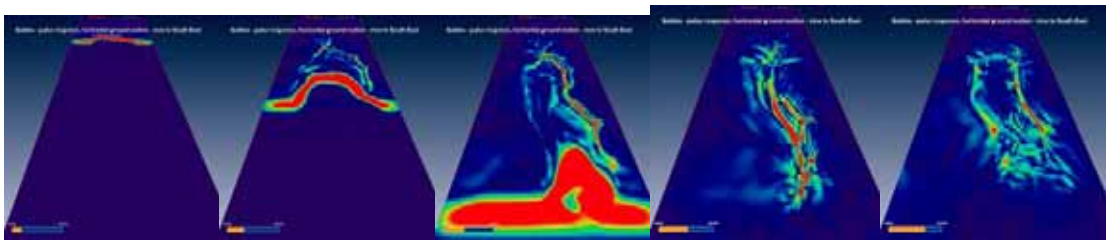

Figure 7.13 Snapshots of peak ground displacement during the 1997 Umbria-Marche main (09:40 UTC, Mw=6.0) shock using parameters given in Table 7.2. Significant amplification occurs inside the basin.

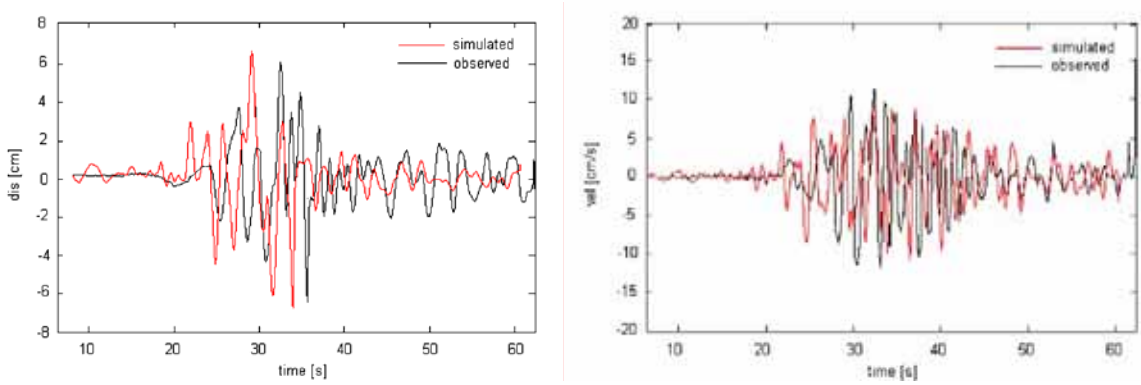

Figure 7.14 3D numerical simulation vs. observation: displacement (left panel) and velocity time history (right panel) for EW component obtained at station GBP for the M6.0 event on 26/09/1997, 09.40 UTC.

7.5 References

Akkar S, Bommer JJ (2007b) Prediction of elastic displacement response spectra in Europe and the Middle East. Earthquake Engineering & Structural Dynamics 36(10): 1275-1301.

Bindi, D., Luzi, L., Massa, M. and Pacor, F. (2009) "Horizontal and vertical ground motion prediction equations derived from the Italian Accelerometric Archive (ITACA)," submitted to Bull. Earth. Eng.

Boncio, P. and Lavecchia, G. (2000) "A structural model for active extension in Central Italy," Jour. Geodynamics, 29, 233-244.

Boore, D.M. and Atkinson, G.M. (2008) "Ground-Motion Prediction Equations for the Average Horizontal Component of PGA, PGV, and 5%-Damped PSA at Spectral Periods between 0.01 s and 10.0 s," Earthquake Spectra, 24 (1), 99-138.

Cauzzi, C. and Faccioli, E. (2008) "Broadband (0.05 to 20 s) prediction of displacement response spectra based on worldwide digital records," Journal of Seismology, DOI 10.1007/s10950-008-9098-y

Hernandez B, Cocco M, Cotton F, Stramondo S, Scotti O, Courboulex F Campillo M (2004) "Rupture history of the 1997 Umbria-Marche (Central Italy) main shocks from the inversion of GPS, DInSAR and near field strong motion data," Annals of Geophysics 47: 1355-1376.

Mirabella F, Ciaccio M G, Barchi M R Merlini S (2004) "The Gubbio normal fault (Central Italy): geometry, displacement distribution and tectonic evolution," Journal of Structural Geology, 26, 2233-2249.

Orsâl, I., J. Brokesová, D. Fäh, D. Giardini (2002): "3D hybrid ray-FD and DWN-FD seismic modeling for simple models containing complex local structures", Stud. Geophys. Geod. 46, 711-730

Pucci, S, De Martini, M., Pantosti, D. and Valensise, G. (2003) "Geomorphology of the Gubbio basin (Central Italy): under standing the active tectonics and earthquake potential," Annals of Geophysics, 46 (5), 837-864.

Project S3 DPC-INGV 2004-2006– Scenari di scuotimento in aree di interesse prioritario e/o strategico; Task 6 –Geological model of the Gubbio Basin (Italy) for the characterization of local seismic response, Deliverable D21, July 2007.

Stupazzini M., Paolucci R. and H. Igel, 2009. Near-fault earthquake ground motion simulation in the Grenoble Valley by a high-performance spectral element code". *Bull. Seism. Soc. Am.*, Vol. 99(1): 286-301.

8. Conclusions and considerations on the future work

A considerable amount of research work has been carried out in the first year of activity of Project S4, referring to the identification in ITACA of stations with distinctive features of seismic response, that should be pointed out for a better qualification and use of the records.

This work encompasses various subjects and approaches, including:
- calibration of new ground motion prediction equations;
- statistical study of strong ground motions on a station-per-station basis;
- detailed geo-morphological analysis using GIS techniques;
- installation of seismic networks for monitoring activity in several carefully selected sites;
- advanced 3D numerical simulations of complex source and site effects in seismic wave propagation.

After the first year of the Project, the results of these studies are still preliminary, but some of them are at an advanced stage of development and are expected to provide soon material for publication in international journals. On the other side, the problem of how to make a synthesis of such results suitable for the goals of the database is being presently faced. A first step in this direction has been the insertion within the station monographs of a space where the "Distinctive features of site response" emerged from this study will be shortly summarized.

Finally, it should be noted that this deliverable has been mostly prepared before the M_w 6.3 L'Aquila earthquake of Apr 6, 2009, that is expected to provide a huge amount of information useful for the progress of this work. Therefore, many results presented in this Deliverable should be tested and possibly improved in view of the earthquake occurrence, while the research activities will be forcedly redirected to encompass the enormous interest raised by this earthquake. Namely:

- the analysis of strong motion records from the RAN and temporary networks installed in the epicentral region just after the mainshock, that will help understanding the seismic response of the Aterno Valley, particularly at the AQK station (L'Aquila Aquilpark), that was already identified as a station with clear amplification effects at long periods and de-amplification at short periods, features confirmed during the L'Aquila seismic sequence (Figure 8.1);

- the updated calibration of the EGMPE described in this report, based on the new records, that better constrain now the short distance range;

- the analysis of L'Aquila earthquake records at sites selected for monitoring within this project, i.e., the Fucino and Norcia basins and the Narni topography, all of them lying at few tens of km distance from the epicenter (Figure 8.2);

- the 3D numerical simulation of wave propagation in the Aterno Valley by the spectral element method, coupling earthquake source and basin effects

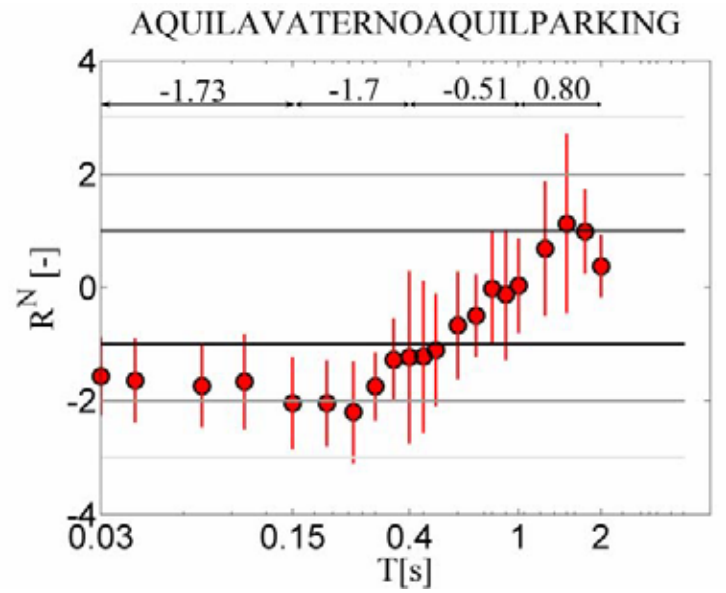

Figure 8.1 Average residual values at AQK station with respect to the median of the EGMPE of Bindi et al (2009), see Chapter 3.3, calculated before the L'Aquila earthquake.

Figure 8.2 Epicenter of L'Aquila earthquake and location of the temporary seismic network installed within Project S4..

9. Relevance for DPC and/or for the scientific community

This deliverable is the scientific basis for improvement of qualification of stations and records of the ITACA database. More generally, the careful analysis of ITACA stations and strong-motion records coming out from this work will provide the reader and the ITACA end-user a comprehensive picture of the problems related to earthquake ground motion analysis and prediction in Italy, that is not usually available for other large strong motion networks throughout the world.

10. Changes with respect to the original plans and reasons for it

No changes with the respect to the original plans occurred during the first year of the project.

11. Key publications

Bindi D., Luzi L.; Pacor F., 2009. Inter-event and inter-station variability computed for the Italian Accelerometric Archive (ITACA). *Bull. Seism. Soc. Am.*, in press.

Bindi D., Luzi L., Pacor F., Sabetta F., Massa M., 2009. Towards a new reference ground motion prediction equation for Italy: update of the Sabetta-Pugliese (1996), *Bull. Earthq. Eng.*, accepted.

Bindi D., Luzi L., Massa M., Pacor F. Horizontal and vertical ground motion prediction equations derived from the Italian Accelerometric Archive (ITACA), *Bull. Earthq. Eng.*, submitted.

Di Alessandro, C., F. Bonilla, A. Rovelli, O. Scotti, 2009. Predominant-period site classification for predictive equations of response spectra in Italy, *Bull. Seism. Soc. Am.*, submitted.

Ditommaso R., M. Mucciarelli, M. R. Gallipoli, F. C. Ponzo, 2009. Effect of a single vibrating building on free-field ground motion: numerical and experimental evidences, *Bull. Earthq. Eng.*, in press.

Gallipoli M.R. and M. Mucciarelli, 2009. Comparison of Site Classification from VS30, VS10, and HVSR in Italy, *Bull. Seism. Soc. Am.*, Vol. 99, No. 1, pp. 340–351

Stupazzini M., Paolucci R. and H. Igel, 2009. Near-fault earthquake ground motion simulation in the Grenoble Valley by a high-performance spectral element code". *Bull. Seism. Soc. Am.*, Vol. 99(1): 286-301.

Annex A – Legenda of Table_Task4.xls

Table_Task4.xls, provided as an electronic supplement available at the Project web site (esse4.mi.ingv.it) with this Deliverable, contains a synthesis of results obtained in the first year of Project S4, concerning the seismic classification of the stations, and the identification of stations with distinctive features, based on the analyses illustrated in Chapters 3, 4 and 5 of this Deliverable. For each station, the following information is provided, where avalaible:

- column A: station code
- column B: latitude (WGS84)
- column C: longitude (WGS84)
- column D: station name
- column E: altitude (meters above the sea level)
- column F: soil classification based on geological maps (1:100000)
- column G: soil class based on Sabetta & Pugliese (1996) classification. This is the soil classification used for deriving the empirical attenuation relationship ITA08 (see Section 2.2) and used in the residues-based method described in Section 3.3.
- column H: Vs30 when available
- column I: proposed classification obtained merging the information, deriving both from geological maps (1:100000) and available measures (see Column L)
- column K: number of available earthquake recordings
- column L: available data for site classification according to SP96 (HVSR=Horizontal to Vertical Spectral Ratios; CH=Vs profile; GEO=surface geology)
- column M: the asterisk denotes those stations located on deep closed-shaped basins, see Chapter 4, where amplification of long period ground motion is likely to occur.
- Columns N to Q: normalized residues (in terms of units of standard deviations σ) obtained with the procedure illustrated in Section 3.3. Results as subdivided into four period ranges: 1) $0.03 \leq T \leq 0.15$ s; 2) $0.15 < T \leq 0.40$ s; 3) $0.40 < T \leq 1.0$ s and 4) $1.0 < T \leq 2.0$ s. stations with residues larger than 1σ are indicated in red
- Columns R to U: normalized residues (in units of σ) computed with the method described in Section 3.2 for the same period bands as above
- Column V: stations with potential directional effects due to station housing (see Table 5.2).